

## BINARY BLACK HOLES IN DENSE STAR CLUSTERS: EXPLORING THE THEORETICAL UNCERTAINTIES

SOURAV CHATTERJEE<sup>1</sup>, CARL L. RODRIGUEZ<sup>1,2</sup>, & FREDERIC A. RASIO<sup>1</sup>

<sup>1</sup>Center for Interdisciplinary Exploration & Research in Astrophysics (CIERA)  
 Physics & Astronomy, Northwestern University, Evanston, IL 60202, USA  
 sourav.chatterjee@northwestern.edu  
 and

<sup>2</sup>MIT-Kavli Institute for Astrophysics and Space Research  
 77 Massachusetts Avenue, 37-664H, Cambridge, MA 02139, USA

### ABSTRACT

Recent  $N$ -body simulations predict that large numbers of stellar black holes (BHs) could remain bound to globular clusters (GCs) at present, and merging BH–BH binaries are produced dynamically in significant numbers. We systematically vary “standard” assumptions made by numerical simulations related to, e.g., BH formation, stellar winds, binary properties of high-mass stars, and IMF within existing uncertainties, and study the effects on the evolution of the structural properties of GCs, and the BHs in GCs. We find that variations in initial assumptions can set otherwise identical initial clusters on completely different evolutionary paths, significantly affecting their present observable properties, or even affecting the cluster’s very survival to the present. However, these changes usually do not affect the numbers or properties of local BH–BH mergers. The only exception is that variations in the assumed winds and IMF can change the masses and numbers of local BH–BH mergers, respectively. All other variations (e.g., in initial binary properties and binary fraction) leave the masses and numbers of locally merging BH–BH binaries largely unchanged. This is in contrast to binary population synthesis models for the field, where results are very sensitive to many uncertain parameters in the initial binary properties and binary stellar-evolution physics. Weak winds are required for producing GW150914-like mergers from GCs at low redshifts. LVT151012 can be produced in GCs modeled both with strong and weak winds. GW151226 is lower-mass than typical mergers from GCs modeled with weak winds, but is similar to mergers from GCs modeled with strong winds.

*Keywords:* black hole physics—methods: numerical—methods: statistical—stars: black holes—stars: kinematics and dynamics—globular clusters: general

### 1. INTRODUCTION

Our understanding of how black holes (BHs) evolve inside star clusters has a long and varied history. Following the classic work by Spitzer (1969), it was suggested that old ( $\sim 12$  Gyr) globular clusters (GCs) cannot retain a significant BH population up to the present day. It was argued that, due to the much higher mass of the BHs compared to typical stars, the BHs will quickly ( $\lesssim 10^2$  Myr) mass segregate to form an isolated subcluster that is dynamically decoupled from the GC. Due to the small size, high density, and small number of objects in the subclusters, relaxation and strong encounters were expected to eject the majority of BHs on a timescale of  $\sim 1$  Gyr. Thus, at most a few BHs would remain in the old GCs observed in the Milky Way (MW, e.g., Kulkarni et al. 1993; Sigurdsson & Hernquist 1993; Portegies Zwart & McMillan 2000; Kalogera et al. 2004). Furthermore, it was argued that if significant numbers of BHs are present in today’s GCs, a subset of them might be in accreting binary systems, and detectable

as X-ray sources. However, observations of luminous X-ray sources in the MW GCs prior to 2012 suggested that *all* of these sources are accreting neutron stars and not BHs, consistent with the theoretical expectation at the time (e.g., van Zyl et al. 2004; Lewin & van der Klis 2006; Altamirano et al. 2010, 2012; Bozzo et al. 2011).

This classical picture started to change with recent discoveries of BH candidates in extragalactic GCs, characterized by their super-Eddington luminosities and high variability on short timescales (Maccarone et al. 2007; Irwin et al. 2010). More recently, with the completion of the upgraded VLA, surveys combining radio and X-ray data for the MW GCs detected quiescent BHs by comparing their radio and X-ray luminosities (e.g., Strader et al. 2012; Chomiuk et al. 2013). Interestingly, the MW GCs containing the detected BH candidates show large ranges in structural properties, indicating that the retention of BHs may be quite common. Several recent or ongoing surveys promise much richer observational constraints on this question (e.g., Strader et al. 2013; Strader 2014; Miller-Jones et al. 2014a,b).

To be detectable either via electromagnetic signatures or via gravitational waves (GW) from BH–BH mergers, the BHs must be in binary systems with very specific ranges of properties. Although dynamical interaction can enhance the production of binaries containing a BH (BBHs) (e.g., [Kundu et al. 2002](#); [Pooley et al. 2003](#)), modern simulations find that the fraction of BHs in binaries is typically low (e.g., [Morscher et al. 2015](#); [Leigh et al. 2014](#)). Hence, it has been argued that detection of just a few BH candidates in GCs indicates the existence of a much larger population of BHs that are not detectable (e.g., [Strader et al. 2012](#); [Umbreit 2012](#); [Morscher et al. 2013, 2015](#)). Indeed, recent numerical studies have found that BH ejection is not nearly as efficient as was previously thought. In these studies, it has been shown that the BH subcluster does not stay decoupled from the rest of the cluster for prolonged periods. The same interactions that eject BHs from the subcluster also cause it to expand and re-couple with the rest of the cluster, dramatically increasing the timescale for BH evaporation (e.g., [Breen & Heggie 2013](#); [Morscher et al. 2015](#); [Wang et al. 2016](#)). These simulations suggest that tens to thousands of BHs may remain in today’s GCs (e.g., [Mackey et al. 2008](#); [Moody & Sigurdsson 2009](#); [Aarseth 2012](#); [Morscher et al. 2013, 2015](#)).

Most recently, [Morscher et al. \(2015\)](#) showed that the presence of a significant number of BHs can dramatically alter the overall dynamical evolution of GCs. Through repeated cycles of core-collapse and core re-expansion, BH-dynamics acts as a significant and persistent source of energy. On the other hand, the clustered environment and high frequency of strong scattering interactions, especially involving binaries, can change the numbers and properties of BBHs that form inside clusters (e.g., [Rodriguez et al. 2015, 2016a](#); [Antonini et al. 2016](#)). Both of these aspects intricately depend on several physical processes, many of which lack strong observational constraints. For example, the distribution of the natal kicks the BHs receive can control how many of them will be directly ejected from the GCs immediately upon formation. Natal kicks also control the fraction of BHs that may retain their binary companions after SN. The high end of the stellar initial-mass function (IMF) determines how many BHs a cluster can form. The binary fraction and binary orbital properties can alter the binary stellar evolution of a BBH (or their progenitors) as well as the rate at which they take part in dynamical encounters. In addition, the ratio between the BH mass and the average stellar mass, also directly set by the IMF, determines the timescale for BHs to sink to the center. Answers to a wide variety of questions, such as how many BHs and BBHs can a GC retain at present, how many BBHs it can form over its whole lifetime, at what rate do BHs and BBHs get ejected from the clusters, and how do the BHs affect the overall evolution of the clusters, can potentially depend on these initial assumptions. Hence, we must understand the sensitivity of our models to initial conditions and assumptions that are poorly constrained

by existing observations.

In this study, we vary the initial assumptions affecting the high-mass stars and BHs, that are usually considered “standard” in theoretical studies of clusters, within their observational uncertainties. In particular, we vary the stellar IMF, the birth-kick distribution for the BHs, and the primordial binary fraction and the binary properties for massive stars. We also vary the assumed prescription for mass loss via stellar winds. Furthermore, we vary the galactocentric distance ( $r_G$ ) and metallicities. Starting from otherwise identical initial star clusters, we study how varying these assumptions affect BH populations, and the overall evolution and final observable properties of the host clusters. We also study how these initial assumptions affect the number and properties of merging BH–BH binaries. We put these findings in the context of the recent landmark detections of GWs from BH–BH mergers by Advanced LIGO ([Abbott et al. 2016d,a,c,e,b](#)).

In §2 we describe our numerical models and we list the initial assumptions that we vary. In §3 we define how we evaluate observable cluster properties from our models. In §4 we show how the various assumptions affect the overall evolution and final observable properties of star clusters. §5 focuses on how these assumptions and resulting differences in the cluster evolution as a whole alter the binary properties of BHs. In §6 we focus on the numbers and properties of BH–BH mergers and put those results in the context of the recent discoveries of GWs ([Abbott et al. 2016d,c,b](#)). We summarize our results and conclude in §7.

## 2. NUMERICAL MODELS

We use our Hénon-type ([Hénon 1971](#)) Cluster Monte Carlo (CMC) code, developed and rigorously tested in our group over the past 15 years ([Joshi et al. 2000, 2001](#); [Fregeau et al. 2003](#); [Umbreit et al. 2012](#); [Pattabiraman et al. 2013](#); [Chatterjee et al. 2010, 2013a,b](#)). For a detailed description of the most recent updates and parallelization see [Pattabiraman et al. \(2013\)](#) and [Morscher et al. \(2015\)](#). The Monte Carlo approach is more approximate than a direct  $N$ -body integration (e.g., [Aarseth 2010](#)), but requires only a fraction of the computational time. This rapidity allows us to fully explore the parameter space of dense star clusters. Results from CMC have been extensively compared to recent state-of-the-art  $N$ -body simulations, and were found to produce excellent agreement in all quantities of interest in this study ([Rodriguez et al. 2016c](#)).

### 2.1. Standard Assumptions

In order to understand the influence of each initial assumption on the production and subsequent evolution of BHs in a cluster, we anchor our numerical models using the same assumptions as used in [Morscher et al. \(2015\)](#). We call this our “standard” model and denote it as S (Table 1, 2). Our standard model initially has  $N = 8 \times 10^5$  stars. The position and velocities of the

stars are set according to a King profile with  $W_0 = 5$  (King 1962, 1965, 1966). We adopt the commonly-used IMF presented in Kroupa (2001), and use the central value for each slope in the different mass ranges between  $0.1$ – $100 M_\odot$  to assign masses to these stars. In model S we assume an initial binary fraction  $f_b = 0.05$ . This is realized by randomly selecting the appropriate number ( $N_b = N \times f_b$ ) of stars, independent of their masses or positions in the cluster, and assigning binary companions to them. The mass of the secondary ( $m_s$ ) is drawn from a uniform distribution with a lower limit taken from the assumed IMF,  $m_{\min} = 0.1 M_\odot$ , and an upper limit equal to the mass of the primary ( $m_p$ ). The orbital period ( $P$ ) is drawn from a distribution flat in  $\log P$  between 5 times the sum of the radii for the binary companions, and the local hard–soft boundary given by  $v_{\text{orb}} = v_\sigma$ , where,  $v_{\text{orb}}$  is the orbital velocity and  $v_\sigma$  is the local velocity dispersion. Note that, although all initial binaries are locally hard, dynamical evolution can make them soft at a later time, either by increasing the local velocity dispersion of other stars (typically in the core) or by moving the binary from its initial location to where the velocity dispersion is higher (due to mass segregation). Such soft binaries are maintained in all our simulations until strong scattering encounters disrupt them. The initial orbital eccentricities for the binaries are drawn from a thermal distribution.

Single and binary stellar evolution is performed with SSE and BSE (Hurley et al. 2000, 2002). We have modified the prescription for stellar remnant formation in SSE and BSE by using the results of Fryer & Kalogera (2001) and Belczynski et al. (2002). All core-collapsed neutron stars get birth kicks drawn from a Maxwellian distribution with  $\sigma = \sigma_{\text{NS}} = 265 \text{ km s}^{-1}$ . We assume momentum ( $|\vec{p}|$ ) conserving kicks for BHs following the prescription of Belczynski et al. (2002). BHs formed via the direct collapse scenario do not get any natal kicks, since there is no associated explosion or mass loss. BHs formed with significant fallback get natal kicks calculated by initially sampling from the same kick distribution as the neutron stars, but reduced in magnitude according to the fractional mass of the fallback ( $x_{\text{fb}}$ ) material (see Morscher et al. 2015, for a more detailed description of our standard model S).

Below we describe how we vary the above-mentioned initial assumptions. In each case we describe only the assumptions we change relative to the baseline model S, with all other initial conditions held constant.

## 2.2. Initial Binary Fraction and Binary Properties of Massive Stars

One source of uncertainty in setting up the initial conditions is whether the binary fraction depends on the stellar mass. We create two models, F0 and F1, varying the fraction of high-mass stars ( $> 15 M_\odot$ ) that are initially in binaries ( $f_{b,\text{high}}$ ). In models F0 and F1, we adopt limiting initial values of  $f_{b,\text{high}} = 0$  and 1, respectively (Table 1, 2). We assign the binaries in these

two models such that the overall binary fraction  $f_b$  is kept fixed at 0.05. In model F0,  $N_b = 0.05 \times N$  stars are randomly chosen from all stars with mass  $\leq 15 M_\odot$  and are assigned as binaries. In model F1, we first assign all stars with mass  $> 15 M_\odot$  as binaries. We randomly choose the appropriate residual number of low-mass stars ( $\leq 15 M_\odot$ ) and assign them as binaries to make  $f_b = 0.05$ . In F0 and F1, the distributions for the mass ratios ( $q$ ) and the orbital properties are identical to model S.

In addition to the binary fraction in high-mass stars, the binary orbital properties can potentially affect both the formation and interaction rate of BHs in a cluster. The observed distributions of initial separations and  $q$  for binaries may have significant uncertainties and selection biases. To understand the effects of these initial assumptions, we create a set of models where we vary the initial binary properties of the high-mass ( $> 15 M_\odot$ ) stars. In these models, we assume that the initial  $f_{b,\text{high}} = 0.7$  following the observational constraint provided in Sana et al. (2012). In addition, we choose an initial period distribution described by  $dn/d \log P \propto P^{-0.55}$  for the high-mass stars (Sana et al. 2012). The number of binaries for low-mass stars are again adjusted so that the overall  $f_b$  is  $\approx 0.05$ , similar to model S. We denote these models with “F0.7.” Within this variant, we also consider two different  $q$  distributions for the high-mass binaries. In one, we use a uniform distribution of  $q$  between  $q = m_{\min}/m_p$  and 1. These models are denoted with the string “Ms0.1”. Another set of models uses the same uniform distribution in  $q$ , but within a much smaller range, 0.6 and 1. We denote this set of models with the string “q0.6” (Table 1, 2).

## 2.3. Natal Kick Distribution for Black Holes

It has been widely accepted that the neutron stars get large natal kicks when they form via core-collapse SN (e.g., Cordes et al. 1993; Lyne & Lorimer 1994; Wang et al. 2006; Zuo 2015). However, the magnitudes of natal kicks imparted to BHs, is still a matter of debate. Observational constraints come from modeling the kicks required to explain the positions and velocities of known BH X-ray binaries (XRB) in the MW galactic potential. Detailed analysis of individual BH XRBs results in widely varying constraints on their natal kick magnitudes (e.g., Brandt et al. 1995; Nelemans et al. 1999; Willems et al. 2005; Gualandris et al. 2005; Dhawan et al. 2007; Fragos et al. 2009; Wong et al. 2012, 2014). Instead of modeling individual systems, Repetto et al. (2012) and Repetto & Nelemans (2015) have performed population synthesis using different assumptions of natal kick distributions and compared their results with the positions of the observed BHs in the MW. They have found that BHs may get large kicks, perhaps even as large as the neutron stars formed via core-collapse SN. In addition, they have not found evidence of a mass-dependent kick distribution, which would be expected

for the widely used  $|\vec{p}|$ -conserving kick prescription. Recent theoretical study of core-collapse SN by [Pejcha & Thompson \(2015\)](#) also suggests that the birth kicks may not be directly correlated with the BH mass. In short, the distribution of formation kicks for BHs is largely uncertain, even at the qualitative level.

In addition to the one used in **S**, we create models with three different natal kick distributions for the BHs. These models assume that the kick magnitudes are independent of the BH masses and  $x_{fb}$ , and are drawn from a Maxwellian given by  $\sigma = \sigma_{BH}$ . We adopt three variations that are obtained by using  $\sigma_{BH} = \sigma_{NS} = 265 \text{ km s}^{-1}$  (denoted by the string “K1”),  $\sigma_{BH} = 0.1\sigma_{NS}$  (denoted by the string “K2”), and  $\sigma_{BH} = 0.01\sigma_{NS}$  (denoted by the string “K3”) in Table 1, 2.

#### 2.4. Initial Stellar Mass Function

A lot of observational effort is aimed towards finding the expected IMF for stars born in clusters (e.g., [Kroupa & Boily 2002](#), and the references therein). Of course, the number of BHs a cluster can form is directly dependent on the number of massive BH-progenitor stars it initially contains. This, in turn, is directly dependent on the stellar IMF, especially the power-law slope of the IMF near the high-end of stellar masses. As described earlier, our standard models use the central values for the IMF slopes from [Kroupa \(2001\)](#). However, we note that the best-fit power-law exponents  $\alpha$  in  $dn/dm \propto m^{-\alpha}$  throughout all mass ranges have large uncertainties. For example, the power-law exponent  $\alpha_1$ , for stars more massive than  $1 M_\odot$  is 2.3 with  $1\sigma$  error of 0.7 ([Kroupa 2001](#)). We vary  $\alpha_1$  within the quoted  $1\sigma$  uncertainties, and create models with  $\alpha_1 = 1.6$  (denoted using the string “If”) and  $\alpha_1 = 3$  (denoted using the string “Is”) in Table 1, 2.

#### 2.5. Stellar Wind Prescription

The details of how stars lose mass to stellar winds is complicated and hard to model theoretically. Most stellar evolution prescriptions instead model the mass and metallicity-dependent stellar winds by calibrating the wind-driven mass loss to catalogues of observed stars (e.g., [de Boer et al. 1997](#); [Van Eck et al. 1998](#); [Hurley et al. 2000](#); [Vink et al. 2001](#)). The assumed wind prescription dramatically affects the mass of the BH progenitor at the time of SN, which in turn determines the mass of the resultant BH. The wind prescription described in [Hurley et al. \(2000\)](#) is widely used as part of the SSE and BSE software packages in many widely-used cluster dynamics codes. The majority of our models use this stellar wind prescription. For simplicity, we call BSE’s implementation for winds as the “strong wind” prescription.

Recent observations of high-mass stars suggest that the stellar winds may not be as strong as suggested by earlier studies (e.g., [Vink et al. 2001](#); [Vink 2008](#); [Belczynski et al. 2010a,b](#); [Dominik et al. 2012](#); [Spera et al. 2015](#)). The details of this wind prescription, based on,

e.g., [Vink et al. \(2001\)](#) is documented in detail in [Belczynski et al. \(2010b\)](#), and implemented in our code in ([Rodriguez et al. 2016a](#)). For simplicity, we call this implementation the “weak wind” prescription. All models adopting weak winds are denoted with the string “W” in Table 1, 2.

#### 2.6. Other Assumptions

In addition to the above variations to our standard model **S**, we also vary the galactocentric distance ( $r_G$ ), metallicity ( $Z$ ), the initial virial radius ( $r_v$ ), and the overall spread in the stellar IMF for a handful of models.

For easier understanding of the variations of initial assumptions in specific models we name all models in a way that specific strings in the name would indicate specific variations. In Table 1 we summarize the specific strings in model names and what they mean. All model names are created using some combination of these strings indicating combinations of specific initial assumptions. The details of all models and initial assumptions are listed in Table 1.

**Table 1.** Naming convention for models

String	Meaning for initial property variations
<b>s</b>	Our baseline model; we use “standard” assumptions for BH kicks, galacto-centric distance, IMF, $f_b$ , and $Z$ ( <a href="#">§2.1</a> ).
<b>Rx</b>	Galacto-centric distance is varied; $r_G = x \text{ kpc}$ ( <a href="#">§2.6</a> ).
<b>z</b>	Metallicity is the same as in the baseline model, $Z = 0.001$ , independent of the galacto-centric distance of the cluster ( <a href="#">§2.6</a> ). In contrast, in other cases, we assume $Z$ is anti-correlated with $r_G$ and assign metallicities consistent with the observed MW GCs at a given galacto-scentric distance ( <a href="#">Djorgovski &amp; Meylan 1994</a> ).
<b>fb0.1</b>	Overall initial binary fraction is changed from our fiducial value, $f_b = 0.05$ , to $f_b = 0.1$ without changing the distributions of initial binary orbital properties.
<b>rv1</b>	Initial $r_v = 1 \text{ pc}$ in contrast to our fiducial value of $r_v = 2 \text{ pc}$ .
<b>Iw</b>	Wider range ( $0.08$ – $150 M_\odot$ ) in the IMF is used relative to our fiducial range ( $0.1$ – $100 M_\odot$ ).
<b>Fx</b>	Binary fraction for high-mass ( $> 15 M_\odot$ ) stars $f_{b,\text{high}} = x$ while keeping the overall binary fraction $f_b = 0.05$ , the same as in the baseline model.
<b>Ms0.1</b>	Minimum secondary mass for initial binaries is $0.1 M_\odot$ . In addition, the initial period distribution is taken from <a href="#">Sana et al. (2012)</a> .
<b>q0.6</b>	Minimum secondary mass for initial binaries is determined such that the mass ratio $q = m_s/m_p \geq 0.6$ . In addition, the initial period distribution is taken from <a href="#">Sana et al. (2012)</a> .
<b>Ki</b>	BH natal kicks are independent of fallback fraction and remnant mass. Index $i=1, 2, 3$ denote $\sigma_{BH}/\sigma_{NS} = 1, 0.1$ , and $0.01$ , respectively.
<b>Is</b>	Steep power-law exponent is used ( $\alpha_1 = 3$ ) for the IMF for stars more massive than $1 M_\odot$ .
<b>If</b>	Flat power-law exponent is used ( $\alpha_1 = 1.6$ ) for the IMF for stars more massive than $M_\odot$ .

*Table 1 continued*

Table 1 (*continued*)

String	Meaning for initial property variations
W	Weak winds (Vink et al. 2001) are assumed.

NOTE—We give informative names to our models. The names are combinations of several strings where each string refers to particular initial assumptions. To aid the readers understand the initial assumptions for particular models directly from the model’s name we list specific strings in the names of our models and their corresponding meaning for the initial assumptions.

### 3. DERIVATION OF OBSERVED CLUSTER PROPERTIES

The definitions for key structural properties in numerical models are often different from those defined by observers for real clusters (e.g., Chatterjee et al. 2013b). To be consistent, we “observe” our simulated models to extract structural properties with definitions similar to those used for real observations. We use the last snapshot from all our model clusters to extract the observable structural properties. All relevant final structural properties, measured both using theoretical definitions, and observers’ definitions are listed in Table 3.

#### 3.1. Estimation of “Observed” Structural Properties

We create two-dimensional projections for each model assuming spherical symmetry. The half-light radius,  $r_{hl,obs}$ , is then estimated by finding the projected radius containing half of the total light. We obtain the observed core radius,  $r_{c,obs}$ , and the observed central density,  $\Sigma_{c,obs}$ , by fitting an analytic King model to the cumulative stellar luminosity at a given projected radius including stars within a projected distance of  $r_{hl,obs}$  from the center (King 1962, their Eq. 18). This method was suggested earlier by Morscher et al. (2015). Since, this approach avoids binning of data, this is more robust against statistical fluctuations, especially at low projected distances compared to the often-used method of fitting the King profile directly to the surface brightness profile (SBP).

We estimate the observed central velocity dispersion  $v_{\sigma,c,obs}$  by taking the standard deviation of the magnitudes of the three-dimensional velocities of all luminous stars (excluding compact objects) within a projected distance of  $r_{c,obs}$ . In case of binaries, we take into account the center of mass velocities.

#### 3.2. Estimation of Dissolution Times

Depending on initial assumptions, some of our cluster models get tidally disrupted before the integration stopping time of 12 Gyr. The basic assumptions of our Monte Carlo approach are spherical symmetry, and a sufficiently large  $N$  to ensure that the relaxation timescale is significantly longer than the dynamical timescale. Both assumptions break down for clusters that have begun to tidally disrupt, since the tidal

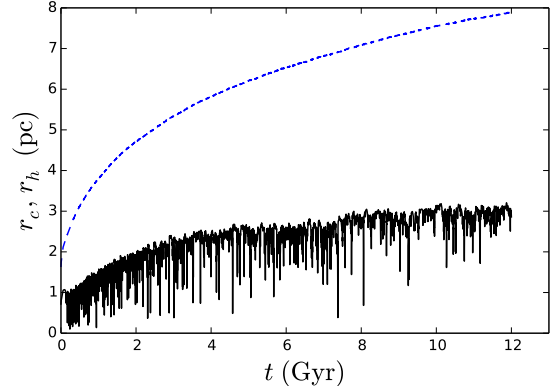


**Figure 1.** Evolution of the core radius ( $r_c$ ) and the half-mass radius ( $r_h$ ) for model S. The solid (black) and dashed (blue) lines denote  $r_c$  and  $r_h$ , respectively. The spikes in  $r_c$  due to BH-driven core collapse continue until the end of the simulation at 12 Gyr. Both  $r_c$  and  $r_h$  expand all the way to the end.

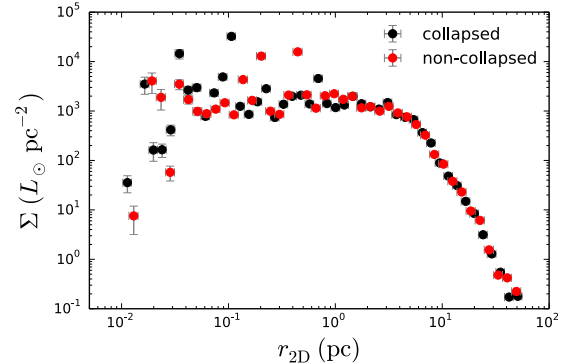


**Figure 2.** Comparison between the SBPs at two different times, one corresponding to a core-collapsed state, seen as the downward spikes in Fig. 1 (at  $t = 9.27$  Gyr; black), and the other corresponding to a non-collapsed state (at  $t = 9.29$  Gyr; red) for model S. The theoretically defined core radius changes from  $r_c \approx 0.4$  during the collapsed state to about 3 pc out of that collapse. However, the observable SBP barely changes.

boundary is not spherically symmetric, and a disrupting cluster can lose mass on a timescale  $<<$  than the relaxation time. To that end, once  $t_r(t) > M(t)/\dot{M}$  for a cluster, where  $t_r$ , and  $M$  denote relaxation time and total cluster mass respectively, we consider the cluster to have dissolved. For clusters that dissolve before 12 Gyr, we list the approximate dissolution times and mark them as “Dissolved” in Table 3.

## 4. OVERALL CLUSTER EVOLUTION

Fig. 1 shows the evolution of the core radius ( $r_c$ ) and the half-mass radius ( $r_h$ ) for our standard model S. As expected,  $r_c$  shows repeated downward spikes indicating collapse of the BH subcluster (e.g., Morscher et al. 2015). Dynamical ejections and binary formation following each BH-driven core collapse produces energy, reversing the collapse and re-expanding the BH posi-

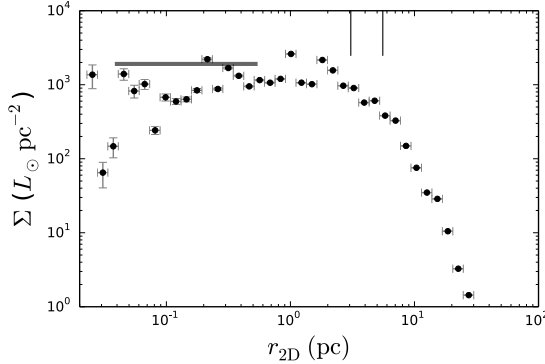


**Figure 3.** Final SBP at  $t = 12$  Gyr for model S. The dots denote the surface luminosity density. While calculating the SBP, we discard stars brighter than  $20 L_\odot$  to reduce noise from a small number of bright giant stars (e.g., Noyola & Gebhardt 2006). The horizontal line denotes the central surface luminosity density ( $\Sigma_{c,\text{obs}}$ ) based on the best-fit King model (83). The vertical lines denote the observed core radius  $r_{c,\text{obs}}$  (obtained from the King fit) and observed half-light radius  $r_{hl,\text{obs}}$ .

tions to mix with the rest of the cluster. Through repeated collapses, the  $r_c$  increases on an average until the integration is stopped at 12 Gyr, and attains  $r_c = 2.8 \pm 0.1$  pc. The error-bar here denotes the  $1\sigma$  fluctuations during the last 1 Myr of the cluster’s evolution.  $r_h$  monotonically increases as well, attaining a final value of about 8 pc.

Of course, an astronomer observing this cluster would measure different values for the structural quantities. Since the core collapse at any time during the evolution involves only a small number of the most massive BHs in the cluster, the observable SBP is insensitive to these collapses. For example, Fig. 2 shows the SBPs for the same model cluster at two different times during its evolution, one when the cluster is in a core-collapsed state and the other when the cluster is out of it. There is no difference between the SBPs, although the theoretical  $r_c$  changes from about 0.4 to 2.8 pc, between the collapsed and non-collapsed states. Thus, the core collapses driven by BH dynamics in these clusters are not observable.

Fig. 3 shows the SBP including stars with luminosity  $L_\star \leq 20 L_\odot$  for model S at  $t = 12$  Gyr. At this time model S has  $\Sigma_{c,\text{obs}} \approx 2.7 \times 10^3 L_\odot \text{pc}^{-2}$ ,  $r_{hl,\text{obs}} = 5.5$  pc, and  $r_{c,\text{obs}} = 3$  pc. Hence, to an observer S would appear as a cluster with low central density and puffed-up core.

In general, if a large number of BHs remain bound to the host cluster, dynamics involving BHs (dynamical formation of new binaries, binary-single and binary-binary scattering, and dynamical ejections from the cluster core) acts as the dominant source of energy in the core. The cluster can start the relaxation-driven core-contraction phase only after this source of energy is sufficiently depleted. The larger the number of retained BHs ( $N_{\text{BH}}$ ) at a given time, the bigger the  $r_{c,\text{obs}}$  and  $r_{c,\text{obs}}/r_{hl,\text{obs}}$  for the host cluster (Fig. 4). For example,

excluding the disrupted clusters, the correlation coefficient between  $N_{\text{BH}}$  and  $r_{c,\text{obs}}$  at  $t = 12$  Gyr is 0.82 and that between  $r_{c,\text{obs}}/r_{hl,\text{obs}}$  is 0.78. Because of the large amount of energy BH-driven dynamics can inject into the clusters, the central density,  $\Sigma_{c,\text{obs}}$ , also depends strongly on  $N_{\text{BH}}$ ;  $\Sigma_{c,\text{obs}}$  and  $N_{\text{BH}}$  are anti-correlated with a correlation coefficient of -0.3 (Fig. 5).

Note that due simply to the differences in the initial assumptions affecting the high-mass stars, clusters with very similar initial conditions attain widely varying final properties spanning  $\sim 4$  orders of magnitude in  $N_{\text{BH}}$ ,  $\gtrsim 2$  orders of magnitude in  $r_{c,\text{obs}}$ , and  $\gtrsim 4$  orders of magnitude in  $\Sigma_{c,\text{obs}}$  at  $t = 12$  Gyr (§2; Tables 2 & 3).

We find that the most dramatic differences in the overall final properties of a star cluster come from the differences in  $N_{\text{BH}}$ . The variations in initial assumptions can change the evolution of  $N_{\text{BH}}$  in different ways, and as a result, change the overall evolution of the cluster and its structural properties (e.g.  $r_{c,\text{obs}}$ ,  $r_{hl,\text{obs}}$ , and  $\Sigma_{c,\text{obs}}$ ). We find that the most important assumption that determines the evolution of  $N_{\text{BH}}$  in a cluster is the natal kick distribution for the BHs. Hence, we start by discussing the effects of initial assumptions related to BH-formation kicks.

#### 4.1. Effects of the Natal Kick Distribution for BHs

The assumed natal kick distribution for BHs directly controls  $N_{\text{BH}}$  at a given time, and through that it controls the evolution of the cluster. For example, Fig. 6 shows the evolution of  $N_{\text{BH}}$ ,  $r_c$ ,  $r_h$ ,  $r_c/r_h$ , and the final SBPs for four identical models, all at a fixed  $r_G = 8$  kpc. These models vary only in the assumed distribution of natal kicks for the BHs. We find that if the BHs are given full NS kicks, i.e.,  $\sigma_{\text{BH}} = \sigma_{\text{NS}}$ , most of the BHs are ejected from the cluster within  $t \approx 20$  Myr, immediately after formation. Without the source of energy from BH dynamics at the center, the cluster starts contracting due to two-body relaxation after the initial expansion from mass loss via stellar evolution. At about 11 Gyr the cluster reaches the so-called binary-burning phase, when core-contraction is arrested due to extraction of binding energy from binary orbits via super-elastic scattering encounters (e.g., Heggie & Hut 2003). Based on the final SBP, this cluster would appear as a high-density core-collapsed cluster (Fig. 6; see also Chatterjee et al. 2013b). In contrast, clusters modeled with other natal kick distributions, where the BHs essentially receive much lower kicks compared to the neutron stars formed via core-collapse SN, do retain large numbers of BHs all the way through 12 Gyr. Due to the energy produced from BH dynamics, each of these clusters continues to expand till the end. K2 with  $\sigma_{\text{BH}} = 0.1\sigma_{\text{NS}}$  contains about 200 BHs at  $t = 12$  Gyr, a sufficient number to keep the cluster in an expanded state. However, the rate of expansion is lower compared to models S and K3 where at 12 Gyr,  $N_{\text{BH}}$  are much higher, with values 464 and 759, respectively. While near the end there are indications that the model cluster K2 would start con-

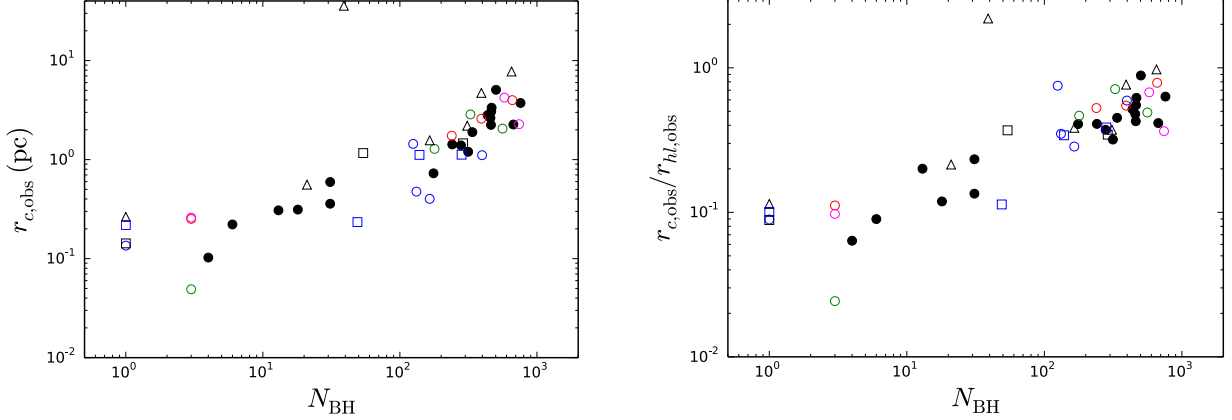


**Figure 4.** Final number of BHs bound to the cluster,  $N_{\text{BH}}$  vs  $r_{c,\text{obs}}$  (Left) and  $r_{c,\text{obs}}/r_{hl,\text{obs}}$  (Right) for all models that survived for at least 11 Gyr. Filled black circles represent models with  $r_G = 8$  kpc,  $r_v = 2$  pc and strong winds. Blue, green, red, and magenta empty circles denote models with the same assumptions for  $r_v$  and stellar wind, but with  $r_G = 1, 2, 4$ , and 20 kpc, respectively. Black triangles denote models with  $r_G = 8$  kpc,  $r_v = 2$  pc, and weak winds. Black and blue squares both denote models with  $r_G = 8$  kpc,  $r_v = 1$  pc, and a wider IMF, but with weak and strong winds, respectively. In general, the larger the  $N_{\text{BH}}$ , the higher the  $r_{c,\text{obs}}$  and  $r_{c,\text{obs}}/r_{hl,\text{obs}}$ . Effects of all other initial assumptions are minor (Table 2). One model is a clear outlier with a very large  $r_{c,\text{obs}}$  and moderate  $N_{\text{BH}}$ : this is model **WIfK1** (Table 3), which is on the verge of dissolution.

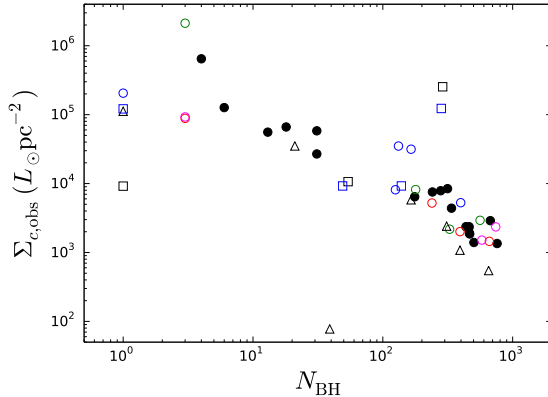


**Figure 5.**  $N_{\text{BH}}$  vs  $\Sigma_{c,\text{obs}}$  for all models that survive for at least 11 Gyr. Point styles are the same as in Fig. 4. The final  $\Sigma_{c,\text{obs}}$  is strongly dependent on  $N_{\text{BH}}$ . Effects of  $r_v$ ,  $r_G$ ,  $f_{b,\text{high}}$  and winds are minor, only effecting  $\Sigma_{c,\text{obs}}$  through  $N_{\text{BH}}$  that are bound in the clusters at 12 Gyr. Model **WIfK1** is on the verge of dissolution and exhibits very low density and moderate  $N_{\text{BH}}$ .

tracting after it ejects some more BHs, models S and K3 are still expanding at  $t = 12$  Gyr, and appear as puffy, low-density clusters from their final SBPs. The same initial cluster can evolve to a final observational state with  $r_{c,\text{obs}}$  and  $\Sigma_{c,\text{obs}}$  varying by orders of magnitude, simply because of changes in the assumed natal kick distribution for its BHs (Table 3).

The significant number of retained BHs can also expand the cluster closer to its tidal radius, making the cluster more prone to disruption from Galactic tides. For example, with otherwise the exact same properties, at  $r_G = 1$  kpc, clusters with relatively larger  $N_{\text{BH}}$  expand more (e.g. SR1Z and K3R1Z), and dissolve much earlier than 12 Gyr. On the other hand, with the same initial conditions, model clusters with relatively lower  $N_{\text{BH}}$

are safe from tidal disruption even at  $r_G = 1$  kpc (e.g., K1R1, K2R1; Table 3).

In general, the larger the value of  $N_{\text{BH}}$ , the lower the final total mass of the cluster. This is because higher  $N_{\text{BH}}$  expands the cluster more and a more expanded cluster loses more mass due to galactic tides. The exact amount of expansion, mass loss, and the final cluster mass also depends on the metallicity ( $Z$ ) of the cluster, since the metallicity controls the wind-driven mass loss and the resulting mass of the BH population. Higher  $Z$  leads to the formation of lower-mass BHs, and as a result the overall expansion due to BH ejections is reduced. The adopted wind prescription yields a similar effect. While the strong wind prescription leads to a higher mass loss at early times compared to the weak wind prescription, the latter leads to the formation of more massive BHs in a cluster than the former. As a result, the same initial cluster under the weak wind assumption eventually undergoes more expansion when the energy production in the center is dominated by BH dynamics. This increased expansion leads to an increased rate of star loss in models with weak winds compared to those with strong winds which reflects in the final  $N$  in these clusters (Table 3).

#### 4.2. Effects of the Assumed IMF

While for a given IMF the BH natal kick distribution is the dominant factor controlling BH retention and overall star cluster evolution, any change to the IMF, especially for the high-mass stars, can also bring about dramatic differences in how the cluster evolves. By directly controlling both the number of high-mass stars formed in a cluster (hence the number of BHs, stellar evolution driven mass loss), and the average stellar mass, variations in IMF can control the evolution of a cluster and even its survival (Chernoff & Weinberg 1990; Banerjee & Kroupa 2011).

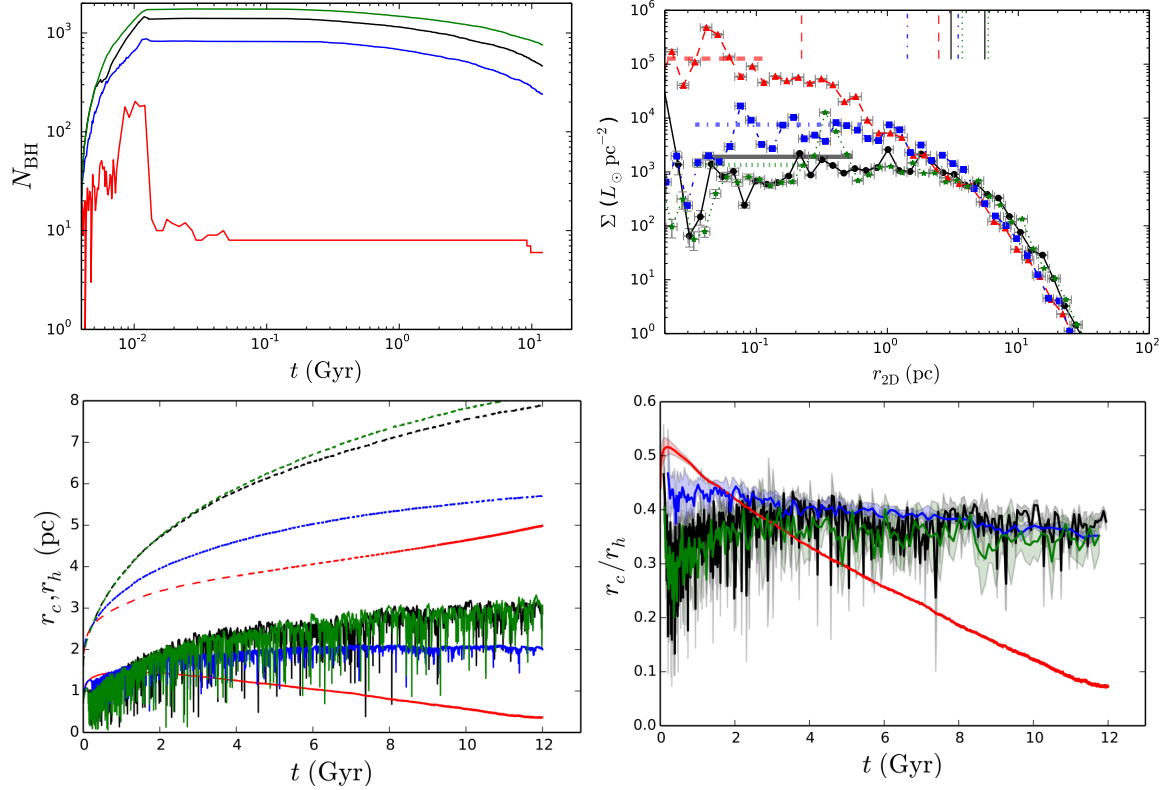


**Figure 6.** Comparison between model clusters S (black), K1 (red), K2 (blue), and K3 (green) (Tables 2, 3) identical except the assumption for the kick distribution during BH-formation. *Top-Left:* Evolution of the bound  $N_{\text{BH}}$  for the four models. *Bottom-Left:* Evolution of  $r_c$  and  $r_h$ . Solid and dashed lines denote  $r_c$  and  $r_h$ , respectively. *Bottom-Right:* Evolution of  $r_c/r_h$ . To reduce scatter we take running averages for  $r_c/r_h$ . The lines denote the mean and the shaded regions show  $1\sigma$  spread. *Top-Right:* Final SBPs for the four models. The horizontal and vertical lines denote  $\Sigma_{\text{c,obs}}$ ,  $r_{\text{c,obs}}$ , and  $r_{\text{hl,obs}}$  for each model. Clearly, the bound  $N_{\text{BH}}$  depends very strongly on the assumed distribution of formation kicks for the BHs. As a result, the overall evolution of the cluster also alters dramatically. For example, K1 with  $\sigma_{\text{BH}} = \sigma_{\text{NS}}$  have only a handful of retained BHs. This cluster evolves to become a dense compact cluster and reaches the binary-burning phase near  $t = 12$  Gyr, with a SBP typical of the so-called core-collapsed observed GCs. In contrast, all other models that retain significantly larger numbers of BHs at  $t = 12$  Gyr, evolve very differently. S and K3 keep expanding until  $t = 12$  Gyr, whereas model K2 ceases to expand at around  $t = 8$  Gyr.

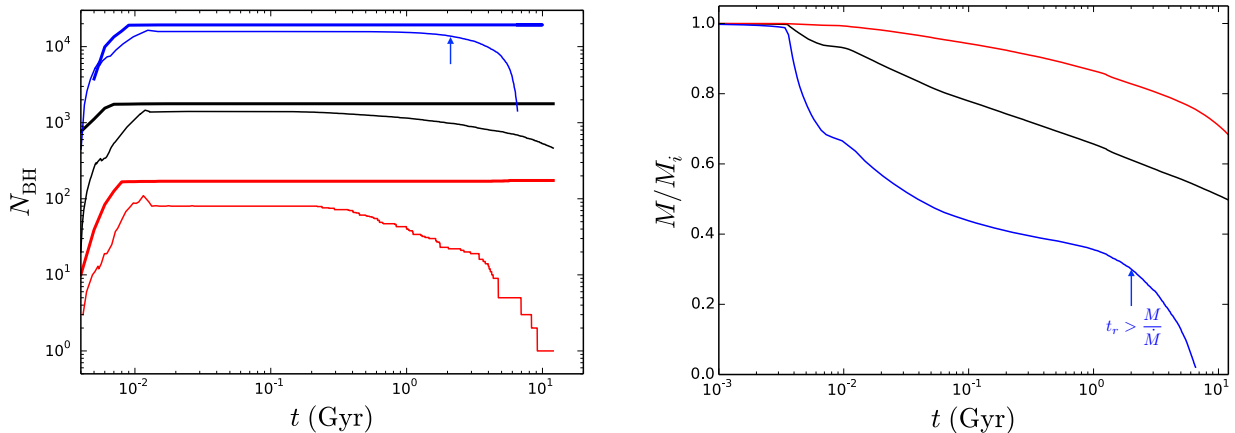


**Figure 7.** Comparison between models with varying IMFs. Each model has a different  $\alpha_1$ , where  $\frac{dn}{dm_*} \propto m_*^{-\alpha_1}$  for  $m_* > 1 M_{\odot}$ . Black (model S), red (model Is) and blue (model If) lines denote  $\alpha_1 = 2.3, 3$ , and  $1.6$ , respectively (see §2; [Kroupa 2001](#)). *Left:* Evolution of the total number of BHs formed (thick lines) and total number of BHs retained by the cluster (thin lines). *Right:* Evolution of the cluster mass normalized to the initial cluster mass. Starting from otherwise identical initial conditions, the three clusters meet with very different fates. The cluster model with  $\alpha_1 = 1.6$  produces many more BHs compared to other models, expands enormously, and gets disrupted around  $t = 2$  Gyr. The approximate disruption time (§3.2) is marked by arrows.

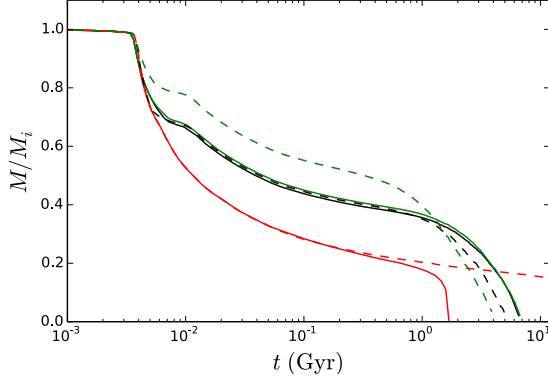


**Figure 8.** Evolution of the star cluster mass normalized by the initial mass of the cluster for models with  $\alpha_1 = -1.6$ . Black, red, and green lines denote models with our standard kick prescription (models **If**, **WIf**), and fallback-independent kick prescriptions with  $\sigma_{\text{BH}} = 1$  (models **IfK1**, **WIfK1**), and  $0.01\sigma_{\text{NS}}$  (models **IfK3**, **WIfK3**), respectively. Solid and dashed lines denote models with strong and weak winds, respectively. All of these clusters get disrupted before  $t = 12$  Gyr. Models that retain significant numbers of retained BHs, weak winds lead to earlier dissolution of the cluster relative to strong winds. Weak winds lead to formation of higher-mass BHs, which lead to faster expansion of the clusters, and correspondingly higher tidal mass loss compared to the strong wind case. For models with  $\sigma_{\text{BH}} = \sigma_{\text{NS}}$ , this is reversed, since in this case with very low values of  $N_{\text{BH}}$ , mass loss from stellar evolution and compact object formation is the dominant effect.

We have tested the effects of variation in the exponent  $\alpha_1$  of the IMF for stars more massive than  $1 M_{\odot}$  within the quoted uncertainty  $2.3 \pm 0.7$  in Kroupa (2001). Clusters evolve very differently depending on the choice of  $\alpha_1$  (Fig. 7). We first focus on our standard set of models (models **S**, **Is**, and **If**; Table 2). While models with  $\alpha_1 = 2.3$  and  $3.0$  evolve normally and survive until  $t = 12$  Gyr, the model with  $\alpha_1 = 1.6$  dissolves at around 2 Gyr (see §3.2 for how dissolution times are estimated). At first, mass is lost primarily via stellar winds. Cluster model **If** loses slightly more mass compared to the other model clusters with steeper  $\alpha_1$ . Dramatic differences appear during the stage when the clusters lose mass via compact object formation. As expected, the steeper the high-end of the IMF, the lower the mass loss from compact object formation. This episode of quick mass loss ends by the time all the BHs are formed and many of the BHs are ejected due to their birth kicks. Following this episode, mass loss slows down and is driven by dynamical ejections of BHs from the core and mass loss through the tidal boundary. At this stage, the number of retained BHs in a cluster becomes very important. A larger value of  $N_{\text{BH}}$  leads to more dynamical ejections, which in turn leads to faster cluster expansion and higher tidal mass loss rate. Eventually, if the cluster expands too much, it gets disrupted.

The details of this process depends both on the kick distribution for the BHs as well as the wind-driven mass loss (Fig. 8). During the initial stages, clusters modeled with weak winds lose less mass than those mod-

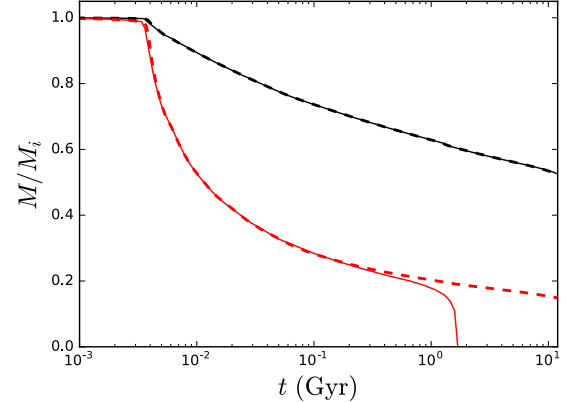


**Figure 9.** Similar to Fig. 8, but for models **K1** (black solid), **WK1** (black dashed), **IfK1** (red solid), and **WIfK1** (red dashed). Since in all models the assumption of  $\sigma_{\text{BH}} = \sigma_{\text{NS}}$  ejects almost all BHs formed in these clusters, dynamical effects of BHs become unimportant. The dominant effect is from mass loss via compact object formation and immediate ejection of most BHs. In models with  $\alpha_1 = 1.6$ , the number of high-mass stars is significantly larger compared to that in models with  $\alpha_1 = 2.3$ . This leads to a much higher mass loss in models **IfK1** and **WIfK1** compared to models **K1** and **WK1**.

eled with strong winds. However, lower wind-driven mass loss leads to the formation of more massive BHs. These higher-mass BHs segregate more rapidly in the cluster potential. In addition, higher-mass BHs inject more energy into the cluster via dynamics and ejections than their lower-mass counterparts. As a result, once the cluster is sufficiently old for BH-dynamics to dominate energy production, the clusters modeled with weak winds expand faster and get disrupted earlier than those modeled with strong winds. The higher the number of retained BHs, the bigger the difference between the clusters modeled with strong and weak winds (Fig. 8). This trend is reversed in the models **IfK1** and **WIfK1**, both modeled with the highest natal kicks for the BHs we consider (Table 2). Since in these models almost all BHs are ejected during formation, the above-mentioned difference due to BH-dynamics is not relevant. Instead, since in the high-kick case, the weak-wind model loses less mass than the strong-wind model, **IfK1** is disrupted earlier than **WIfK1**. To further illustrate this point, Fig. 9 shows the effects of  $\alpha_1$  on models with  $\sigma_{\text{BH}} = \sigma_{\text{NS}}$ . Since most BHs are ejected during formation from all of these models (**K1**, **WK1**, **IfK1**, **WIfK1**) the evolution really depends only on the mass loss from compact object ejections during formation, i.e., the number of high-mass stars formed in the cluster.

#### 4.3. Effects of Other Assumptions

The process and timescale for energy production from BH dynamics depend critically on the mass segregation timescale ( $t_S$ ) in a cluster (e.g., Breen & Heggie 2013; Morscher et al. 2013, 2015). The mass segregation timescale of a massive object depends on the relaxation timescale ( $t_r$ ), and the ratio of its mass to the average stellar mass ( $\langle m \rangle$ ) in its neighborhood,  $t_S \propto t_r \frac{\langle m \rangle}{m_i}$

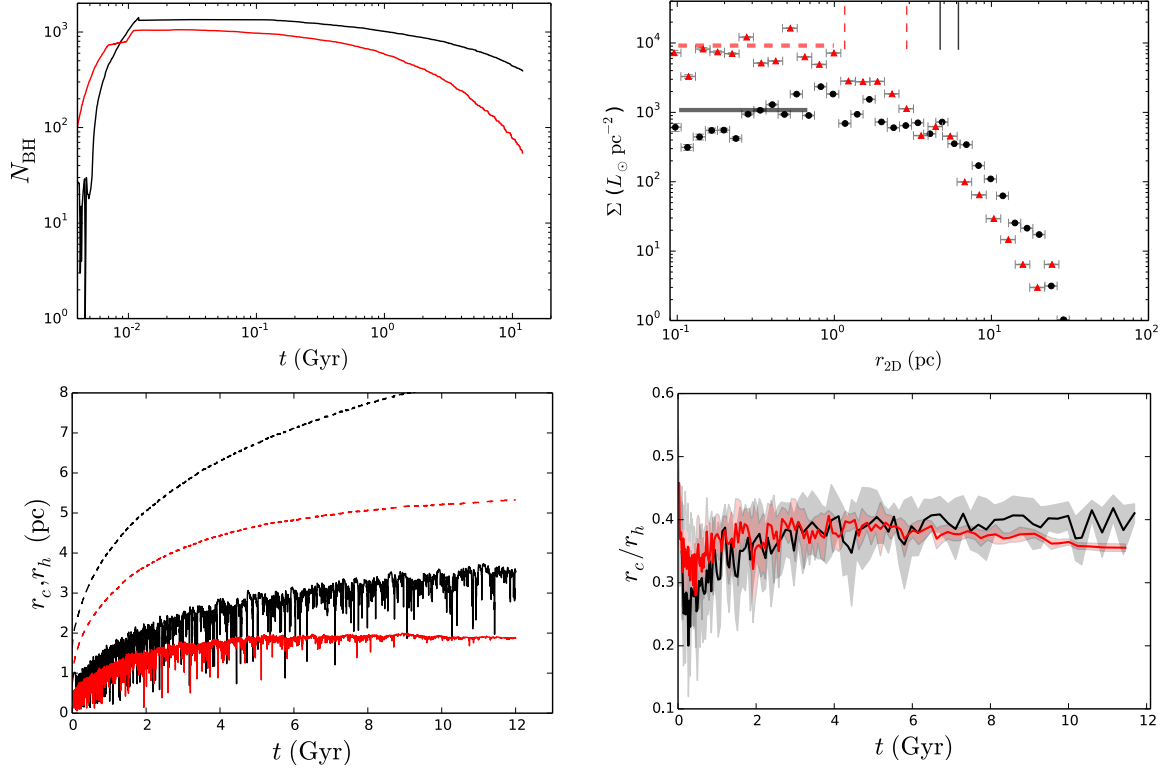


**Figure 10.** Same as Fig. 6, but comparing between models W (black) and Wrv1fb0.1 (red; Table 2). The lower relaxation timescale and average stellar mass for model Wrv1fb0.1 compared to model W leads to faster mass segregation, and as a result faster dynamical processing of BHs. The retained number of BHs  $N_{\text{BH}}$  in model cluster Wrv1fb0.1 is significantly lower compared to  $N_{\text{BH}}$  in model cluster W. As a result, model cluster Wrv1fb0.1 ceases to expand by  $t = 12$  Gyr, and begins the relaxation-driven slow-contraction phase. In contrast, model cluster W keeps expanding till the end. Wrv1fb0.1 appears as a higher-density and more compact cluster compared to W.

(e.g., Gürkan et al. 2004). Thus,  $N_{\text{BH}}$  and as a result, the overall cluster evolution depends on assumptions, such as: initial virial radius ( $r_v$ ), and the IMF, that can affect either  $t_r$  or  $\frac{\leq m \geq}{m_i}$ . Fig. 10 shows the difference in the evolution of two clusters (W and Wrv1fb0.1) with different initial  $r_v$  and the overall spread in the IMF (Table 2). The initial average stellar mass for models W and Wrv1fb0.1 are  $\langle m \rangle = 0.66 M_{\odot}$  and  $0.62 M_{\odot}$ , respectively. The initial half-mass relaxation times for the models are 5.2 Gyr and 1.9 Gyr. Due to these differences, Wrv1fb0.1 processes through its BHs much faster than W. Furthermore, Wrv1fb0.1 retains significantly fewer  $N_{\text{BH}}$ , and evolves to a much denser and more compact final cluster than W.

We have also tested how changes in the binary fraction and binary properties of high-mass stars affect the overall cluster evolution. We find that with a fixed overall  $f_b$ , variations simply in  $f_{b,\text{high}}$  and the distributions of orbital and companion properties for the high-mass binaries do not significantly affect the overall evolution of the clusters and their global observable properties.

## 5. BLACK HOLE BINARIES

To be detectable, either by observation of electromagnetic signals generated via accretion from a non-BH companion in a BH–non-BH binary (BH–nBH), or by

detection of GWs from a BH–BH merger, BHs must be in binary systems. Here we explore the effects of our various initial assumptions on the number and properties of BBHs. Dense star clusters are expected to be efficient factories of dynamically created binary BHs (e.g., Downing et al. 2010, 2011; Kundu et al. 2002; Pooley et al. 2003) although at any given time the binary fraction for BHs inside the cluster remains low due to an ongoing competition between dynamical creation, and disruption and ejection of binary BHs (Morscher et al. 2015). Table 4 lists all our models and the corresponding numbers of single and binary BHs, retained and ejected from each cluster over its lifetime.

### 5.1. Black hole binaries retained in clusters

In general, we find that the number of BBHs (of any kind) in each of our model clusters is much lower compared to the total number of BHs (Table 4). Moreover, the BBH numbers are *not* strongly dependent on  $N_{\text{BH}}$  (Fig. 11). For example, depending on the assumptions in our models, we find a large range in the values of  $N_{\text{BH}}$ , varying from 0 to 935 at  $t = 12$  Gyr. In contrast, at  $t = 12$  Gyr the variation in the numbers of BH–BH ( $N_{\text{BH–BH}}$ ) and BH–nBH ( $N_{\text{BH–nBH}}$ ) binaries are 0 to 7 and 0 to 17, respectively. The correlation coefficient between  $N_{\text{BH}}$  and  $N_{\text{BH–BH}}$  at  $t = 12$  Gyr for all model

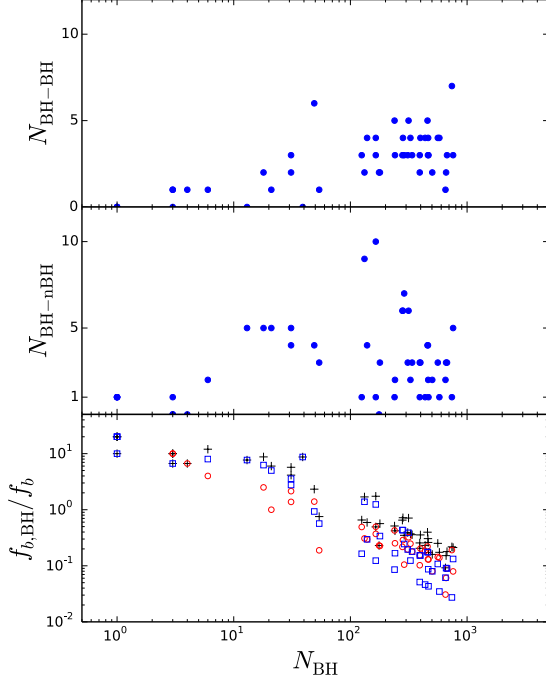


**Figure 11.** *Top:* The number of bound BHs  $N_{\text{BH}}$  vs the number of bound BH-BH binaries  $N_{\text{BH-BH}}$ . *Middle:*  $N_{\text{BH}}$  vs the number of bound BH-nBH binaries  $N_{\text{BH-nBH}}$ . *Bottom:* Binary fraction in BHs ( $f_{b,\text{BH}}$ ) normalized by the overall binary fraction  $f_b$ . Plusses (black), circles (red), and squares (blue) denote the normalized binary fraction for all BH binaries, BH-BH binaries, and BH-nBH binaries, respectively. A larger fraction of BHs are in binaries relative to the overall binary fraction for models with low  $N_{\text{BH}}$ . High  $N_{\text{BH}}$  leads to BH-driven core-collapse which typically disrupts and ejects BH binaries. As  $N_{\text{BH}}$  decreases, BH-driven core-collapses stop occurring, reducing the efficiency of BBH destruction and ejection. BHs being the most massive objects, typically get exchanged into binaries via binary-mediated scattering encounters. As a result, the fraction of BHs in binaries increases as  $N_{\text{BH}}$  decreases.

clusters that did not get disrupted earlier than 12 Gyr is 0.56 and that between  $N_{\text{BH}}$  and  $N_{\text{BH-nBH}}$  is 0.07 (Table 4).

These general trends are understandable from the basic process of how BBHs are created and dynamically processed inside dense star clusters. Almost all primordial binaries containing massive stars are disrupted inside a cluster. This is mainly due to orbital expansion via mass loss, which makes these binaries susceptible to disruption via subsequent strong scattering encounters (Fig. 12). Thus, most BHs in dense star clusters are singles. Almost all BBHs in dense star clusters, as well as BBHs that are ejected from them after  $t \sim 10^2$  Myr, are binaries that are dynamically created in the dense cores of these clusters, and are *not* primordial. Note that even if an old star cluster typical of the present-day GCs now appears to have a low central density, its BHs likely have been processed in dramatically higher density environments as a result of repeated past BH-induced core collapse episodes (e.g., Figs. 1, 3, & 6). Both the values of  $N_{\text{BH-BH}}$  and  $N_{\text{BH-nBH}}$  in a cluster show large fluc-

tuations over time and can vary between zero to  $\sim 10$  (e.g., Figs. 12–15). This is reflective of the high frequency of dynamical processes that create, modify, disrupt, and eject the BBHs in a dense star cluster, especially during a BH-driven core collapse. In these dense environments BBHs continuously form via three-body encounters, change via swapping of partners in binary-mediated scattering, get disrupted via strong scattering, and get ejected due to recoil from strong scattering encounters (e.g., Heggie 1975). The dynamical processes including disruption of primordial binaries, creation of new ones, and dynamical ejections essentially erase the binary properties the high-mass stars were born with. This in fact is the main difference between BBHs formed in a dense star cluster and BBHs that are born in isolation in the field. In the latter case, all BBHs are formed from primordial binaries, hence, the BBH properties as well as numbers relative to single stars are directly related to the assumptions of initial binary properties for the high-mass stars.

While large numbers of BHs are still present in a star cluster, the core of the cluster is dominated by the BHs due to mass segregation. Internal dynamics determines how many of these BHs can hold onto their companions once formed via dynamics. As  $N_{\text{BH}}$  decreases, the BH-driven core collapses become less pronounced. As a result, a higher fraction of BHs can remain in binaries, and the ejection rate of BBHs decreases. Hence, although  $N_{\text{BH}}$  decreases, the fraction of BHs in BH-BH binaries increases, thus keeping  $N_{\text{BH-BH}}$  largely unchanged (Fig 11). On the other hand, while  $N_{\text{BH}}$  is large, the very central regions are dominated by the (mostly) single BHs and lower-mass stars are driven out. A large  $N_{\text{BH}}$  also keeps the cluster puffed up, lowering the rate of encounters between BHs and binaries with non-BH members. Only after a cluster is sufficiently depleted of the BHs, can the rate of formation of BH-nBH binaries via exchange interactions involving a BH and a binary with non-BH members increase. However, at this stage the maximum  $N_{\text{BH-nBH}}$  is likely limited by the low number of remaining BHs.

The lack of a strong correlation between  $N_{\text{BH}}$  and  $N_{\text{BH-nBH}}$  has some interesting implications. For example, major efforts are now underway to detect BH candidates in GCs (e.g., Strader et al. 2012; Chomiuk et al. 2013; Strader et al. 2013; Miller-Jones et al. 2014b,a). For detection via electromagnetic signals (e.g., by comparing the radio and X-ray luminosities) there must be a BH with a non-BH accreting companion. For simplicity, if we treat  $N_{\text{BH-nBH}}$  as a proxy for the absolute upper limit on the number of BH candidates that may be detectable via electromagnetic signatures, the lack of correlation between  $N_{\text{BH}}$  and  $N_{\text{BH-nBH}}$  poses a serious challenge in inferring the number of total BHs in the GC from the discovery of BH candidates in that GC. Note, however, that creation of accreting BHs in star clusters is likely a complex process which requires that the binary is not disrupted for a sufficient time to allow accretion.

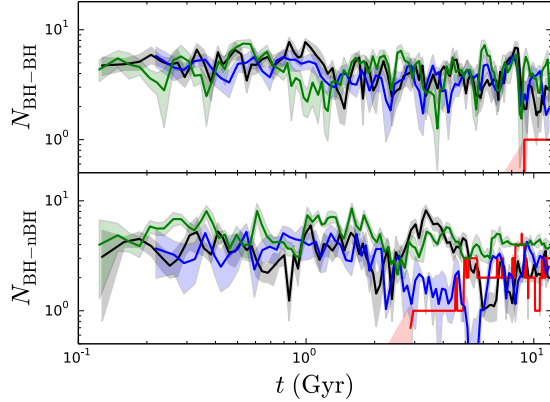


**Figure 12.** Evolution of the number of binary BHs bound to the cluster for different assumed natal kick distributions for BHs. Top and bottom panels show BH-BH and BH-nBH binary numbers. Both  $N_{\text{BH-BH}}$  and  $N_{\text{BH-nBH}}$  show large scatters over time. This is a direct consequence of the continuous disruption and ejection of existing binaries and dynamical formation of new ones at any given time in clusters. To reduce scatter we have under-sampled and show the mean (lines) and  $\pm 1$  standard deviation (shaded region). Black, red, blue, and green denote models S, K1, K2, and K3, respectively (Table 2). Both  $N_{\text{BH-BH}}$  and  $N_{\text{BH-nBH}}$  remain low independent of the assumed distribution of natal kicks for BHs. This indicates that the softening of orbits for massive binaries due to mass loss via winds and compact object formation is responsible for dynamical disruption of most primordial binary orbits, and that this process does not depend on the natal kick distribution. Even with very low adopted natal kicks for BHs,  $\sigma_{\text{BH}} = 2.65 \text{ km s}^{-1}$ , K3 contains low numbers of binary BHs.

Even when this is satisfied, the duty cycle may be low for such accreting binaries (Kalogera et al. 2004). We encourage a more detailed study on this topic.

We now focus our attention on understanding the detailed evolution of BBHs inside a cluster and the effects of various initial assumptions through selected example models (Figs 12–15). Since we have shown that the assumed BH natal-kick distribution can bring dramatic changes to the overall cluster evolution, we first investigate the effects of BH formation kicks on the evolution of BBHs that are retained in the cluster (Fig. 12). The number of BBHs in the cluster is quite insensitive to the details of the kick distribution except for the case with  $\sigma_{\text{BH}} = \sigma_{\text{NS}}$  (e.g., model K1). In the high-kick cases, the large formation kicks essentially eject most of the BHs from the cluster during formation. The natal kicks are also large enough to disrupt all binaries during BH formation. Hence, not surprisingly, in the high-kick models, the values for  $N_{\text{BH-BH}}$  as well as  $N_{\text{BH-nBH}}$  are always low. Interestingly though, the number of BBHs is low even in our lowest kick models. For example, S, which assumes a fallback-dependent momentum-conserving kick prescription and K3, which assumes that  $\sigma_{\text{BH}} = 2.65 \text{ km s}^{-1}$ , typically much lower compared to orbital speeds of the massive binaries, both show low numbers of BBHs. As discussed earlier, the combined mass loss from stellar winds and compact object formation for high-mass stars expands the binary

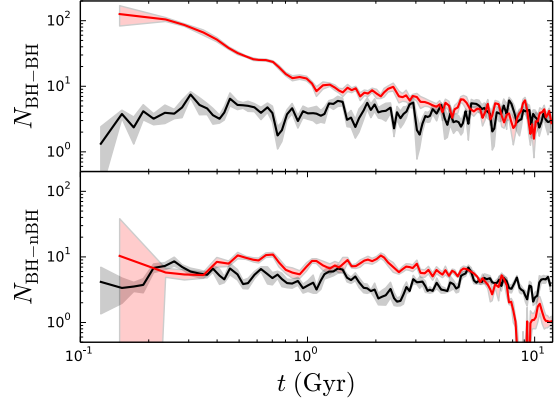


**Figure 13.** Same as Fig. 12 but showing a comparison between the evolution for two identical initial models differing only by the initial binary fraction in high-mass ( $> 15 M_{\odot}$ ) stars,  $f_{b,\text{high}}$ . Black and red denote models F0 with initial  $f_{b,\text{high}} = 0$  and F1 with initial  $f_{b,\text{high}} = 1$ , respectively (Table 2). In both cases, the overall binary fraction  $f_b$  is kept fixed at 0.05. Independent of the initial  $f_{b,\text{high}}$ , the final retained  $N_{\text{BH-BH}}$  converge to a low value. The final retained  $N_{\text{BH-nBH}}$  depends on the efficiency with which interactions involving BHs and binaries with non-BH components can produce BH-nBH binaries via exchange. The cluster with  $f_{b,\text{high}} = 1$  has fewer low-mass binaries than the cluster with  $f_{b,\text{high}} = 0$ . As a result, BH-nBH binary formation is less effective in F1 compared to that in F0 at late times.

orbits and make them dynamically soft. Thus the majority of the high-mass binaries are disrupted independent of the magnitude of the SN kicks. To further investigate this we compare two of our models that are identical in all aspects except the fraction of high-mass stars that are initially in binaries. To illustrate the limiting cases, Fig. 13 shows the evolution of retained BBHs for models F0 with initial  $f_{b,\text{high}} = 0$  and F1 with initial  $f_{b,\text{high}} = 1$  (§2.2; Table 2). Although initially the values of  $N_{\text{BH-BH}}$  are vastly different between the models, within about 3 Gyr, they converge to essentially the same steady value in both models. This further highlights that the number and properties of BH-BH binaries that would be retained in a cluster at late times are set by the internal dynamics and overall cluster properties, and *not* on the details of the initial binary orbital properties, or binary fraction in high-mass stars. The number of BH-nBH binaries,  $N_{\text{BH-nBH}}$ , for the model with initial  $f_{b,\text{high}} = 1$  is slightly lower compared to that in the model with initial  $f_{b,\text{high}} = 0$  for  $t > 5$  Gyr. This is due to the fact that to keep the overall  $f_b$  fixed at 0.05, the  $f_{b,\text{high}} = 1$  case started with fewer low-mass stars in binaries compared to the  $f_{b,\text{high}} = 0$  case. At late times, all BH-nBH binaries are dynamically formed via exchange interactions where a BH inserts itself into a binary by ejecting a non-BH component. Because of this, the relatively small number of low-mass stellar binaries in the  $f_{b,\text{high}} = 1$  case (compared to  $f_{b,\text{high}} = 0$  case) reduces the efficiency of new BH-nBH binary formation.

Independent of how many high-mass stars were born in binaries, cluster dynamics regulates the total num-

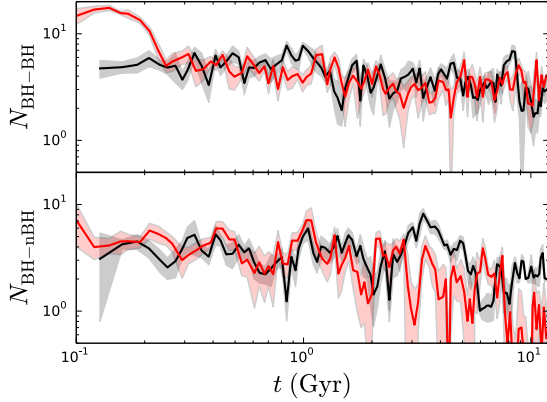


**Figure 14.** Same as Fig. 12 but compares between the evolution for two identical initial models differing by the assumed prescription for mass loss via stellar winds. Black and red denote models **S** with the strong and **W** with the weak wind prescriptions, respectively. The values of  $N_{\text{BH-BH}}$  shows no difference between the two models. The value for  $N_{\text{BH-nBH}}$  for the weak wind case is slightly lower compared to that for the strong wind case. Weak winds lead to more massive BHs, which in turn lead to more expanded clusters with lower central densities (e.g., Table 3). As a result, in the weak wind case, at late times formation of BH-nBH binaries via binary-mediated exchange interactions between single BHs and non-BH binaries is less efficient.

ber of BBHs retained in old GC-like clusters. Other variations in the binary orbital properties and  $f_{b,\text{high}}$  (e.g., Sana et al. 2012) show the same general result. All knowledge of the primordial binary fraction and binary orbital properties of BHs or their progenitors is lost due to dynamical encounters in a star cluster. If massive stars were initially mostly in binary systems, these binaries would take part in strong dynamical encounters with other stars. These frequent scattering encounters either disrupt the binaries or eject them from the cluster. On the other hand, if initially BHs or their progenitors are not in binaries, new binaries can form dynamically. Through both channels the final number of BBHs attains small but similar values in all GCs (e.g., Table 4).

Similar trends are found by comparing models with differing prescriptions for stellar winds (Fig. 14). While the values of  $N_{\text{BH-BH}}$  are very similar between clusters **S** and **W**, the lower final  $\rho_c$  in **W** results in production of a lower number of BH-nBH binaries compared to **S** at late times. This is consistent with our understanding that most BH-nBH binaries retained in old clusters typical of the GCs are dynamically created. The dynamical age, mass-segregation timescale, and the overall binary fraction can also moderately affect  $N_{\text{BH-nBH}}$ . The first two control  $N_{\text{BH}}$  in the cluster, and as a result the cluster’s dynamical properties and overall evolution. The initial binary fraction controls the number of binaries with no BH components that can take part in exchange interactions with single BHs and BH-BH binaries in old clusters. Fig. 15 compares  $N_{\text{BH-BH}}$  and  $N_{\text{BH-nBH}}$  for two models **W** and **Wr1fb0.1** that differ in their initial  $r_v$ , and  $f_b$  (Table 2). While  $N_{\text{BH-BH}}$  converges to similar values within 200 Myr, **Wr1fb0.1** with a higher  $f_b$

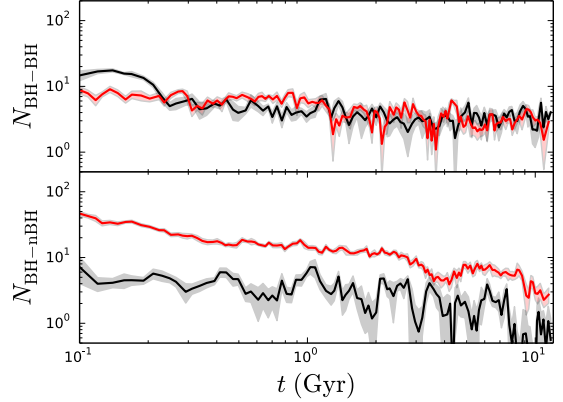


**Figure 15.** Same as Fig. 12 but showing a comparison between the evolution for two models differing by the overall binary fraction,  $r_v$ , and the IMF spread. Black and red denote models **W** and **Wr1fb0.1**, respectively (Table 2). The retained  $N_{\text{BH-BH}}$  for both models converge within  $t \approx 200$  Myr. The model cluster **W** with a lower initial  $f_b$  retains a lower  $N_{\text{BH-nBH}}$  compared to **Wr1fb0.1**. (Tables 2, 4).

creates and retains a larger number of BH-nBH binaries compared to **W**. In all cases, the fraction of BHs that are in binaries increases only after  $N_{\text{BH}}$  is sufficiently reduced (e.g., Fig. 11; also Table 4).

### 5.2. Black hole binaries ejected from clusters

Figure 16 shows the evolution of the number and fraction of BH binaries ejected from model clusters **S**, **K1**, **K2**, and **K3**. There are some noticeable trends in these models which are actually common to all our models. In model **K1**, where we apply high natal kicks to BHs, ejected binary BHs of all types, BH-BH or BH-nBH, have very low values. High natal kicks not only disrupt binaries during BH formation, these high kicks also eject most of the BHs from the cluster during formation (e.g., Figure 6), hence, they never get a chance to dynamically acquire companions. As a result, most of the ejected BHs are singles. Also, the handful of ejected BH binaries leave the cluster at very early times, essentially with the rest of the BHs due to natal kicks. In contrast, in the other models with either fallback-dependent natal kicks (e.g., **S**) or scaled-down natal kicks for BHs (e.g., **K2**, **K3**), a significant number of BHs are retained even after all BHs are formed. In these cases, there are three distinct evolutionary stages. The first sharp rise between few to  $\sim 10$  Myr in the number of ejected BH binaries is coincident with BH formation. These are essentially BH binaries that are ejected from the cluster primarily due to formation kicks. By this time all BHs are already formed. Mass loss from stellar evolution, compact object formation and ejection due to natal kicks have already taken place resulting in significant expansion of the cluster (e.g., Fig. 1). This stage is followed by a flat part, between  $\sim 10$  and 200 Myr. During this time the most massive BHs that are retained in the cluster are in the process of mass segregation. As a result, few BHs,

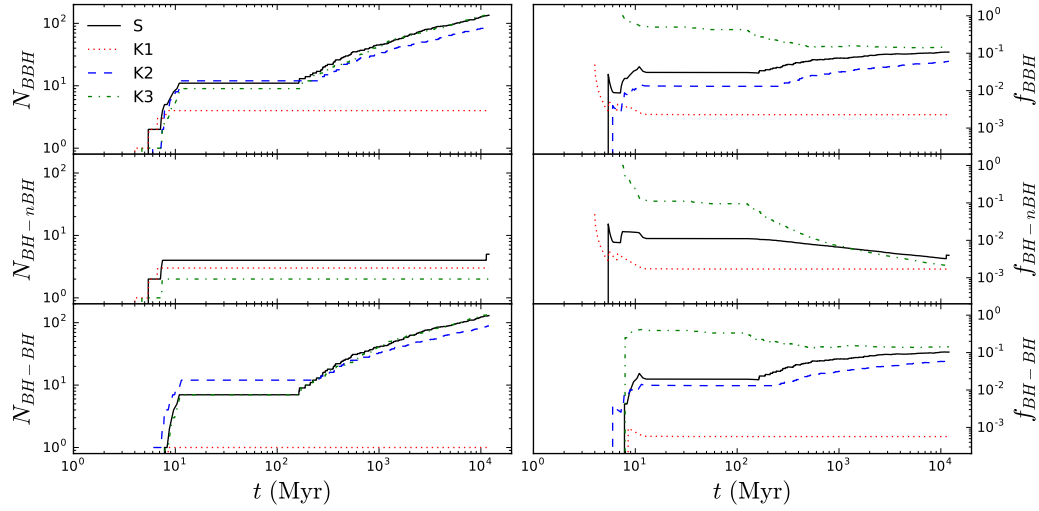


**Figure 16.** Evolution of the number (left) and fraction (right) of ejected binary BHs. Top to bottom, panels show evolution of all binary BHs, BH-nBH binaries, and BH-BH binaries ejected from the cluster vs the cluster age. Black (solid), red (dotted), blue (dashed), and green (dash-dot) denote models S, K1, K2, and K3 (Table 2; §2), respectively. The number of ejected BH-nBH binary stays low in all cases. No BH-nBH binaries were ejected in K2 likely due to statistical fluctuations.

single or binary, are ejected between  $\sim 10$ –200 Myr. A corresponding flat part can also be seen in the evolution of  $N_{\text{BH}}$  (e.g., Figure 6). By  $\sim 200$  Myr the heaviest retained BHs are mass segregated and the BH-driven core-collapse episodes start. During this stage BHs are ejected from the cluster via strong dynamical encounters. BH binaries are also ejected steadily. BH-BH binaries dominate all ejected BBHs in this stage. Most of the BH-nBH binaries are ejected at the early stages primarily due to BH natal kicks. This is an expected consequence of BH mass segregation. BHs dominate the population in the central part where most of the strong binary-mediated encounters take place. Thus, single BHs can easily form new BH-BH binaries. Recoils can eject them from the cluster. In contrast, while a significant number of BHs are retained in the cluster, it is hard to dynamically form or eject a BH-nBH binary simply because the BHs and binaries with non-BH members do not interact as often or as energetically. Thus BH-nBH binaries are not created in large numbers, and when they do form, they are typically retained in the cluster.

Interestingly, the final ejected binary fraction attains very similar values and does not seem to depend on the natal kick distribution, provided that the cluster retains significant numbers of BHs after formation and the BHs get a chance to dynamically evolve inside the cluster for a significant time (Figure 16). Figure 17 shows a similar figure, but comparing models SIwfb0.1 and SIwfb0.1rv1 (Tables 2, 3). Note that in these models the IMF range is different from model S. The qualitative stages for the evolution of the number and fraction of BH binaries are very similar. In addition, the stage of

cluster dynamics driven BH binary ejection starts earlier in the model that is initially more compact ( $r_v = 1$  pc) with respect to the other ( $r_v = 2$  pc). Note that the number of BH binaries ejected via cluster dynamics is about an order of magnitude higher compared to those ejected early due to natal kicks in all cases (Figures 16, 17). This is true in all of our models except in the high-kick cases (models denoted by K1 in their names; Tables 1, 2), where few BHs remain bound to the cluster after their formation.

Since almost all BH binaries are created via dynamical processes, their orbital properties are also set by these dynamical processes, and not the initial assumptions for the binarity or the binary orbital properties of high-mass stars. Figure 18 compares the semimajor axes and eccentricities of ejected BH binaries from four different models, namely S, F1, F0.7Ms0.1, and F0.7q0.6, with widely different assumptions for the initial binary fraction of the high-mass stars, and the initial distributions of their orbital properties (Table 2). Independent of these initial assumptions, the ejected BH binaries, attain very similar orbital properties at the time of ejection from the respective clusters. The general trend for the dynamically ejected BH-BH binaries is an increase of the semimajor axes with time (Figure 18). This is imprinted from the chaotic and repeated dynamical encounters these binaries experience prior to ejection. Once a hard binary forms, subsequent dynamical encounters typically make it harder transferring the excess energy to the center-of-mass velocities of the interacting stars, popularly known as “Heggie’s Law” (Heggie 1975). Since the recoil speed is set by the binary orbital energy, the recoil speed of the increasingly hardening binaries

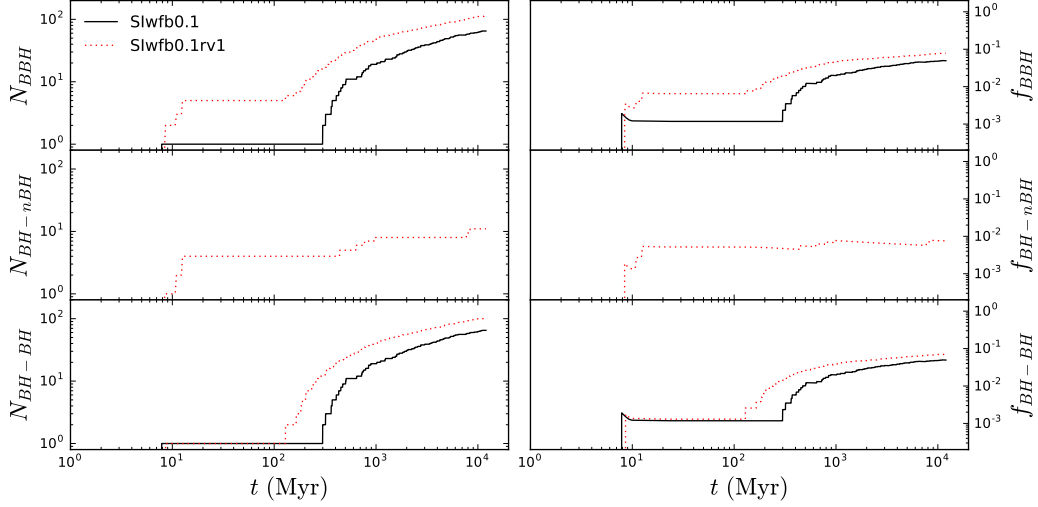


**Figure 17.** Same as Figure 16, but for models **SIwfb0.1** (black solid) and **SIwfb0.1rv1** (red dotted) illustrating differences resulting from the difference in the initial virial radius of the cluster. The qualitative stages in the evolution of the number and fraction of ejected binary BHs are very similar to those shown in Figure 16. Dynamical ejection of BH-BH binaries start earlier in the initially more compact cluster (**SIwfb0.1rv1**) as expected.

increase after each such encounter, until it becomes sufficient to eject the binary from the cluster. Since recoil speeds are set by the binary orbital energy, the orbital energy and hence the semimajor axes of ejected binaries are set by the instantaneous escape speed of the cluster (see Rodriguez et al. 2016a, for a recent in-depth discussion). As the cluster evolves, the escape speed from the cluster’s center becomes lower due to the decrease in the cluster mass and the overall expansion of the core (e.g., Figures 1, 6, 7, 10). Hence, the semimajor axis of typical binaries that are dynamically ejected from the cluster center, increases with time. Note that a competing effect could have been in action. The heavier BHs get ejected earlier. Thus, at earlier times, for a given energy of ejection (and thus binary orbital energy), the binary orbits could be larger. This latter effect does not seem to dominate in our models.

## 6. BINARY BLACK HOLE MERGERS

The BH–BH merger rates and properties of the BHs during merger in the local universe have been studied by multiple teams, either exploring the contributions from star clusters (e.g., Banerjee et al. 2010; Ziosi et al. 2014; Rodriguez et al. 2015, 2016a,b; Antonini et al. 2016; Wang et al. 2016; Chatterjee et al. 2016) or from isolated binary stellar evolution in the field (e.g., Belczynski et al. 2014; Dominik et al. 2012, 2013; Belczynski et al. 2014; Dominik et al. 2015; Kowalska-Leszcynska et al. 2015; Belczynski et al. 2015). Here we focus on understanding the uncertainties associated with the BH–BH merger rates formed in clusters similar to the present-day GCs (e.g., Rodriguez et al. 2016a). We estimate BH–BH merger times using the quadrupole approximate GW orbital evolution equations (Peters 1964). These equations

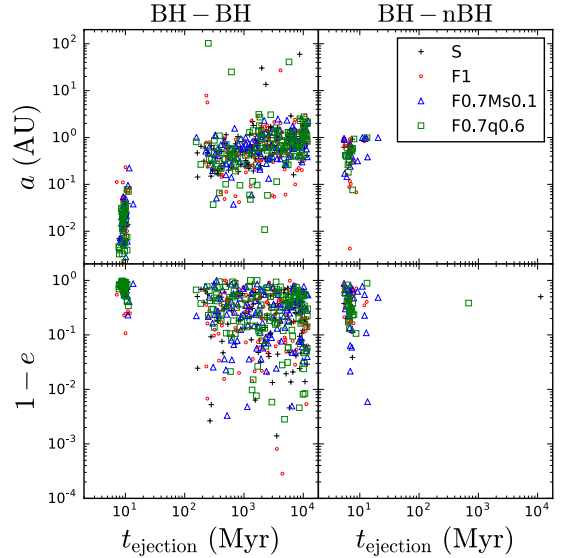


**Figure 18.** Semimajor axis (top) and eccentricity (bottom) at the time of ejection as a function of the ejection time for ejected binary BHs from models **S**(black plus), **F1**(red circle), **F0.7Ms0.1**(blue triangle), and **F0.7q0.6**(green square; Tables 1, 2). Left and right panels are for ejected BH-BH and BH-nBH binaries, respectively. Independent of the initial assumptions for high-mass binary fraction ( $f_{b,\text{high}}$ ), and the binary orbital properties, the ejected binary BHs, especially those ejected at late times due to stellar dynamics, have very similar orbital properties. This bolsters the claim that the orbital properties of ejected binary BHs are set by the dynamical processes inside the cluster center and not by the initial assumptions of orbital properties of the BH-progenitor stars. Since stellar dynamics created these BH binaries, their eccentricities are also typically high.

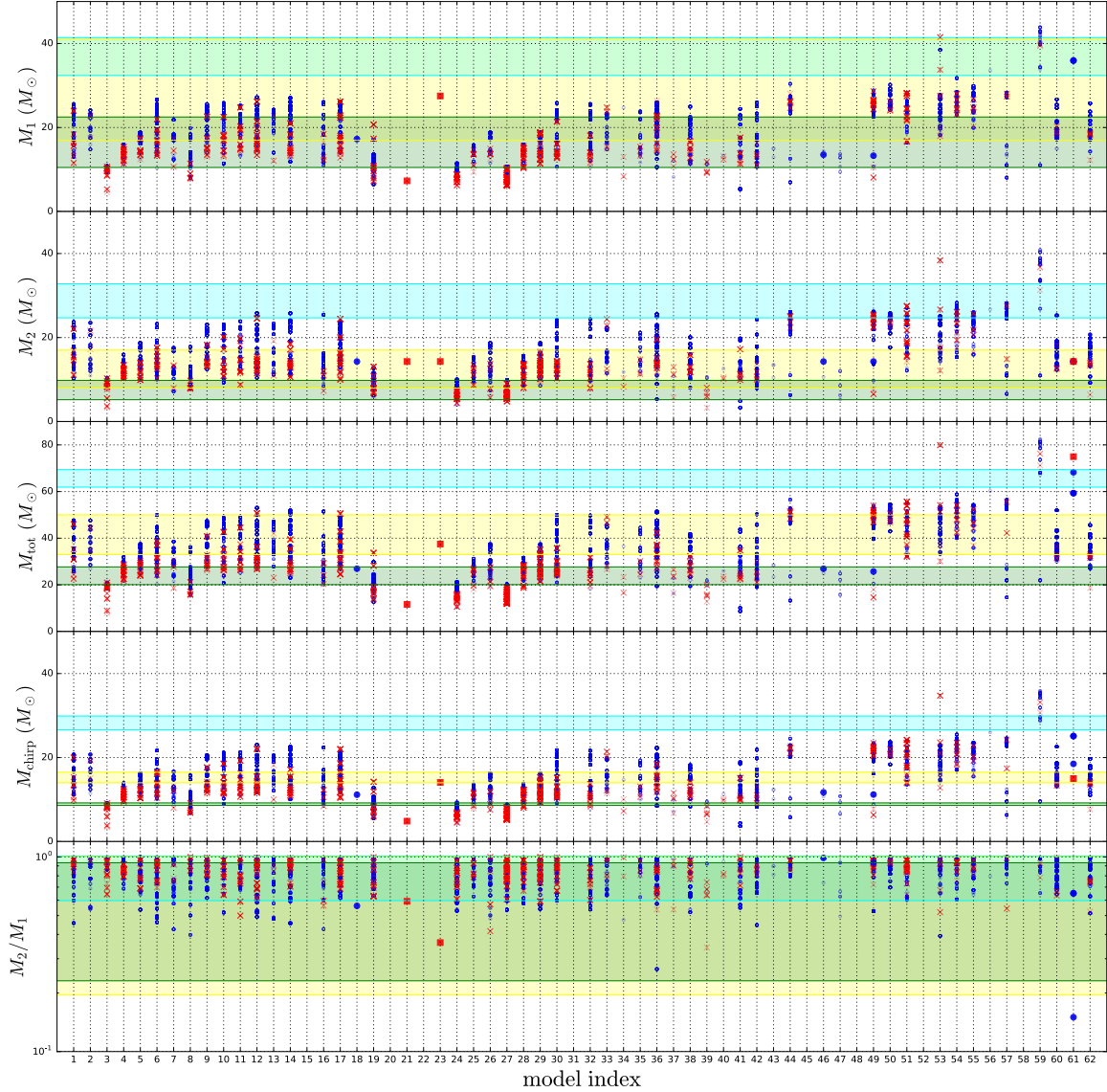


**Figure 19.** Top to bottom, the component masses ( $M_{1,2}$ ), total mass ( $M_{\text{tot}}$ ), chirp mass ( $M_{\text{chirp}}$ ), and mass ratio ( $M_2/M_1$ ) for BH-BH mergers within  $0 > z \geq 0.2$  (blue) and  $0.2 \geq z \geq 1$  (red) for each model identified by the serial numbers on the horizontal axis. Crosses and dots denote in-cluster mergers after being ejected from the clusters. Circles and squares denote mergers within the clusters. Cyan, yellow, and green shaded regions show GW150914, LVT151012, and GW151226 properties for reference (e.g., Abbott et al. 2016b). Weak winds help creating relatively more massive mergers. Assumptions of BH's natal kicks and IMF affect number of mergers by changing the number of BHs that clusters can retain for dynamical processing, and the number of BHs produced for a given  $N$ , respectively.

are applied within BSE for tracking mergers of BH-BH binaries retained in the clusters. We use the same equations to track mergers of the ejected BH-BH binaries using their properties at the time of ejection. We ignore the ejected non-BH binaries at early times which might evolve into BH-BH binaries post ejection since such systems are extremely rare. As in earlier sections, we investigate how variations in initial assumptions affect the number of BH-BH mergers, merger times, and the properties of the binaries. The numbers of BH-BH mergers and the total masses of these mergers within two values of redshift ( $z$ ) are listed in Table 4. Here we assume that each cluster is 12 Gyr old at the present

day, and the redshift corresponds to the lookback time of each merger.<sup>1</sup> To highlight the assumption relating  $t$  and  $z$ , we will refer to our model clusters as GCs in this context. For a detailed analysis of how the assumption of a fixed formation time for all clusters affect the BH-BH mergers within a given redshift see Chatterjee et al. (2016).

Fig. 19 shows the BH masses for all BH-BH mergers within  $z = 0.2$  and 1 from all of our models, identified by

<sup>1</sup> We assume  $h = 0.677$ ,  $\Omega_M = 0.309$ ,  $\Omega_K = 0$ , and  $\Omega_L = 0.691$ .

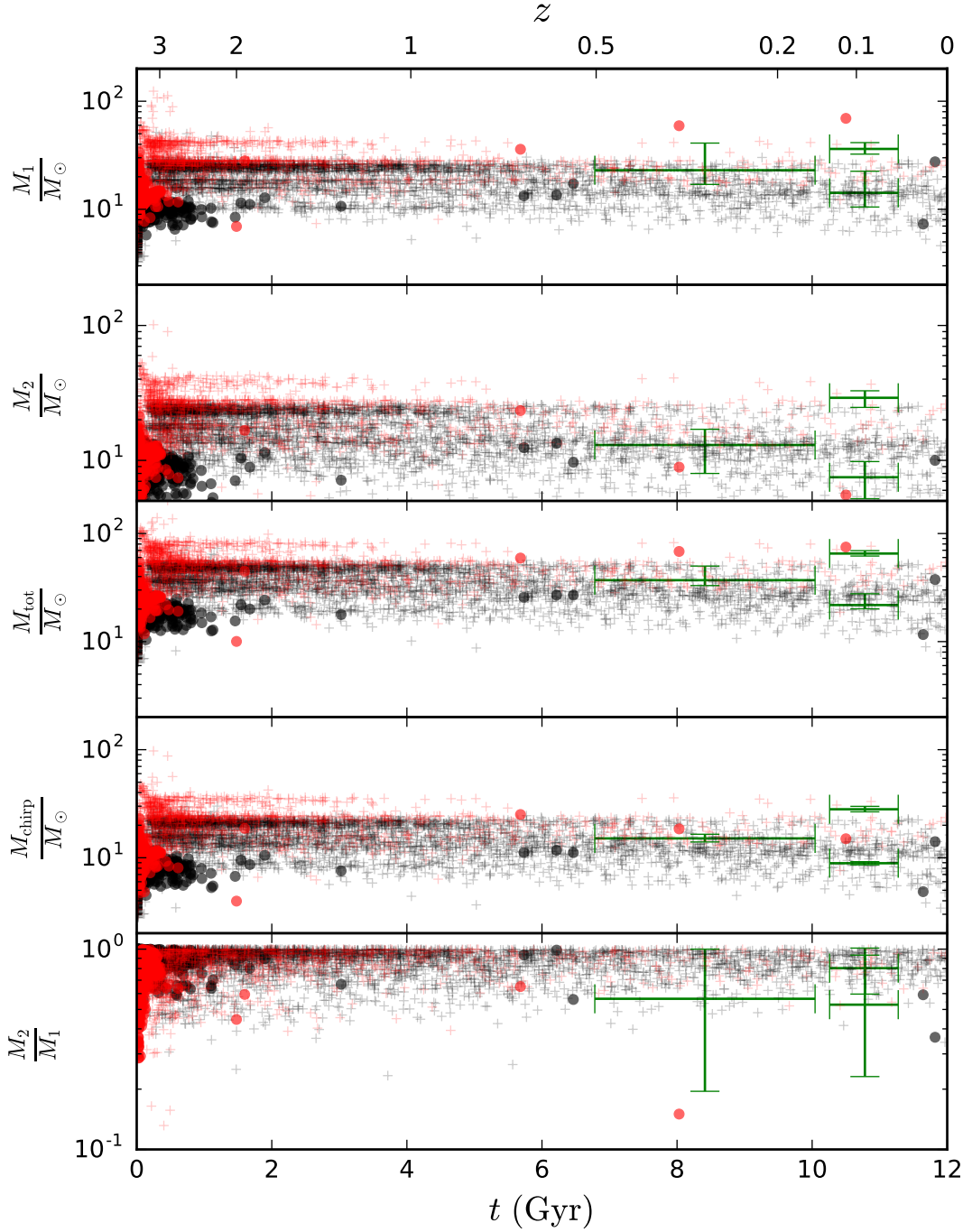


**Figure 20.** Top to bottom, the component masses ( $M_{1,2}$ ), total mass ( $M_{\text{tot}}$ ), chirp mass ( $M_{\text{chirp}}$ ), and mass ratio ( $M_2/M_1$ ) for BH-BH mergers as a function of merger time. The top axis shows the lookback redshift  $z$  assuming that  $t = 12$  Gyr is equivalent to  $z = 0$ . Plusses, and circles denote mergers that happen after the BH-BH binaries are ejected from the host clusters, and BH-BH mergers that happen while the binaries are still bound to the host clusters. The green errorbars show the detected events GW150914, LVT151012, and GW151226 (e.g., Abbott et al. 2016b). Black and red denote BH-BH mergers from models assuming the strong and weak wind prescriptions, respectively. Most BH-BH mergers in the local universe happen after the binaries are ejected from the host clusters. BH-BH binaries that merge inside clusters typically have lower masses compared to those that merge after being ejected. Weak winds are necessary for producing BH-BH mergers as massive as GW150914 for the metallicities we consider. Most mergers in our models are closer in properties to LVT151012.

the index numbers listed in Tables 2–4. Rodriguez et al. (2015, 2016a) found that the BH–BH mergers in the local universe ( $z < 1$ ) is dominated by mergers that occur *after* the BH–BH binaries are ejected from their host GCs. This same result is generally found in our models independent of the details of the initial assumptions (Table 4). Now we highlight the assumptions that affect the number and properties of BH–BH mergers originating from GCs and occurring within some small  $z$ .

The largest effect arises from the assumed distribution of natal kicks for the BHs. We have already seen that independent of initial assumptions, primordial binaries involving BH–progenitor stars are generally disrupted (§5). All GCs modeled with an adopted BH natal kick distribution given by  $\sigma_{\text{BH}} = \sigma_{\text{NS}}$  and no scaling based on fallback, eject almost all of their BHs due to the high natal kicks before they can dynamically form binaries. The handful of BH–BH binaries these GCs produce are all dynamically formed via binary-mediated strong scattering encounters within clusters at later times. As a result, when these GCs do produce BH–BH binaries that would merge in the local universe the mergers usually happen while the BH–BH binary is still bound to the GC.

The only other assumption explored in this study that can significantly impact the production of merging BH–BH binaries from GCs is the IMF. Any variations in the IMF for high-mass stars alters the number of mergers at  $z < 1$  in a predictable manner. IMFs that produce more high-mass stars, produce more BHs, and the number of BH–BH mergers in the local universe increases accordingly. For example, the IMF with  $\alpha_1 = 1.6$ , for a given initial  $N$  forms much higher numbers of BHs compared to models with larger  $\alpha_1$ . Even models with the largest natal kicks for the BHs may produce significant numbers of BH–BH mergers if  $\alpha_1 = 1.6$  is assumed. Of course, for the same reason, a combination of flat high-end for the IMF and low natal kicks for BHs can significantly increase the number of mergers within  $z < 1$ . Nevertheless, note that we find that all clusters modeled with  $\alpha_1 = 1.6$  get disrupted long before they are 12 Gyr old, a typical age for the MW GCs, due to a combination of mass loss and energy production via BH dynamics from the large numbers of high-mass stars that such an IMF produces. As a result, this extreme low value of  $\alpha_1$  seems very unlikely in reality. Similarly, if the IMF mass range is extended to lower-mass stars, the number of BHs produced, and as a result, the number of BH–BH mergers is reduced.

While the distribution of natal kicks and the assumed IMF may change the actual number of BH–BH mergers from GCs within a given  $z$ , the masses of the binary mergers depend on neither. Instead, the mass distribution of the merging BHs is primarily determined by the assumed stellar winds for a given metallicity  $Z$ , which we controlled by using either the weak or strong wind prescriptions in this study (§2.5). Fig. 20 shows the component masses ( $M_{1,2}$ ), total mass ( $M_{\text{tot}}$ ), chirp mass

( $M_{\text{chirp}}$ ), and the mass ratios ( $M_2/M_1$ ) of all BH–BH mergers within 12 Gyr from all our models as a function of their merger times. We divide all model GCs in two groups based on the two wind prescriptions we consider. GCs modeled with weak winds produce more massive BH–BH binaries that would merge within a Hubble time compared to those modeled with strong winds. In particular, GCs modeled assuming weak stellar winds are the only ones that can produce BH–BH mergers with masses similar to GW150914 for the metallicities we consider. Nevertheless, we find that the majority of BH–BH binaries merging within  $z = 0.2$  even from model GCs assuming weak winds and a broader IMF have typically lower BH masses than the component masses of GW150914 (Table 2). Using an even broader IMF would not increase the typical intrinsic mass distributions for BH–BH binaries merging in the local universe for the metallicity we consider. While high progenitor mass, low metallicities, and weak winds help enhance production of high-mass BH–BH binaries, the majority of them merge at high redshifts (Fig. 20) assuming that the parent clusters had formed 12 Gyr ago. Most recently Chatterjee et al. (2016) find that GW150914’s  $M_{\text{chirp}}$  is within  $2\sigma$  of the *intrinsic* distributions for  $M_{\text{chirp}}$  of BH–BH binaries formed in clusters with metallicities lower than  $0.05Z_{\odot}$  and merging within  $z = 0.2$ . Nevertheless, detection of BH–BH mergers as massive as GW150914 may not be as uncommon due to selection effects. For example, Rodriguez et al. (2016b) find that accounting for selection effects,  $M_{\text{chirp}}$  of GW150914 is within  $1\sigma$  of detected BH–BH binaries merging within a redshift of 0.5.

The BH masses of LVT151012 are more common in the BH–BH mergers found in our models. GCs modeled with both strong and weak winds can produce BH–BH mergers similar in properties to LVT151012. The  $M_{\text{chirp}}$  of GW151226 is within the range of masses for BH–BH binaries merging within a redshift of 0.2 from models with strong wind, but is a bit lower compared to those from models with weak winds. Nevertheless, note that many of these conclusions depend on the assumption of the formation time and metallicity of the parent clusters (Chatterjee et al. 2016).

Very few ( $\sim 1\%$ ) of the BH–BH mergers in the local universe are expected to happen while the binary is still bound to the host GC. Most BH–BH binaries that merge while bound to the GC do so at early times, and typically have lower masses than those that merge after ejection. Since, the higher the mass of the BHs, the earlier it is ejected from the cluster (e.g., Morscher et al. 2015), the mergers after ejection are typically more massive compared to those that happen within a cluster.

## 7. SUMMARY AND DISCUSSION

In this study we have explored how identical initial clusters can diverge in their evolution depending on various ill-constrained initial assumptions affecting the high-mass stars, including the high-end slope ( $\alpha_1$ ) of the IMF,

the distribution of natal kicks for BHs, the binary fraction and the binary orbital properties for massive stars, and the prescriptions adopted for stellar winds. Using Monte Carlo simulations we have studied the effects of each of these assumptions from three different perspectives: (1) how they affect the global evolution of star clusters and their final observable properties; (2) how they affect the binary fraction of BHs and the numbers of different types of BH binaries; and (3) how these assumptions affect the number and properties of merging BH–BH binaries that could be detected as GW sources.

We find that, even when we start from the same initial cluster model, variations in these initial assumptions can alter the number of retained BHs,  $N_{\text{BH}}$ , at any given time by orders of magnitude (e.g., Tables 3, 4). This difference in  $N_{\text{BH}}$  can then change the overall dynamical evolution of the host star cluster, dramatically altering its lifetime and, if it survives to the present, its final observable properties (Figs. 4–10).

In contrast, the total number and properties of BH–BH and BH–nBH binaries retained inside old star clusters are not significantly affected by varying any of these assumptions. Through dynamical interactions in the dense cluster cores or kicks at compact object formation, all primordial binaries containing BH progenitors are quickly disrupted. On the relaxation timescale, binaries are reformed dynamically and eventually both the number and properties of retained binaries with at least one BH component are determined entirely by stellar dynamical processes. As  $N_{\text{BH}}$  decreases, the fraction of BHs in binaries increases, so that  $N_{\text{BH–nBH}}$  and  $N_{\text{BH–BH}}$  in old clusters do not strongly correlate with  $N_{\text{BH}}$ . This has important implications for inferring  $N_{\text{BH}}$  in clusters where BH XRB candidates have been identified. In general we find that observable cluster properties including  $r_{c,\text{obs}}$  and  $\Sigma_{c,\text{obs}}$  are better indicators of  $N_{\text{BH}}$  compared to  $N_{\text{BH–nBH}}$  (Figs. 4, 5, & 11).

The number of BH–BH mergers from clusters in the local universe is only affected by the assumptions made about BH natal kicks and the stellar IMF (Fig. 19, Table 4). This is very different from the situation encountered in binary population synthesis studies for field binaries, where a myriad of assumptions (e.g., about the initial properties of binaries) and uncertain stellar evolution parameters (e.g., the infamous common-envelope efficiency  $\alpha_{\text{CE}}$ ) can change results by orders of magnitude. Instead, far more robust theoretical predictions can be made for merging BH–BH binaries that are dynamically produced in dense star clusters.

If BHs receive natal kicks as large as neutron stars formed in core-collapsed SN, the expected number of BH–BH mergers becomes very small, simply because al-

most all BHs are ejected from the cluster at birth. Note, however, that with such large kicks the number of BH–BH binaries generated in star clusters is significantly higher than in the field, where BHs can never again acquire a binary companion if natal kicks disrupt the primordial binaries they were born in (see Rodriguez et al. 2016a, for comparative rate estimates between star clusters and the field assuming high and low natal kicks for BHs). Variations in the assumed IMF slope change the number of BH–BH mergers in clusters in a predictable way, simply by changing the relative proportion of high-mass stars (see §6, Fig. 19). The component masses and total masses (or equivalently the chirp masses) of merging BH–BH binaries are affected only by the assumed prescription for stellar-wind mass loss. Other parameters such as  $f_{b,\text{high}}$  or any of the initial properties of massive binaries (e.g., the distributions of mass ratios and orbital periods) have no effect at all (Fig. 19, Table 4).

In the context of GW detection, we therefore expect the BH–BH merger rates and properties estimated in Rodriguez et al. (2015, 2016a) for dynamically produced binaries to be quite robust, and in particular to remain unaffected by any change in assumptions concerning the initial distributions of binary properties or the binary stellar evolution. In contrast, the BH–BH merger rates estimated for isolated field binaries (e.g., Belczynski et al. 2015; Dominik et al. 2013, 2015) depend directly and sensitively on many assumptions concerning the details of stellar evolution (mass transfer, tidal dissipation effects, common envelopes) and on the assumed distributions of initial properties for high-mass binaries. In addition, the assumption of truly isolated binary evolution may be suspect because most stars and binaries currently in the field were still originally formed in clusters, which later dissolved (e.g., Carpenter 2000; Lada & Lada 2003; Porras et al. 2003; Portegies Zwart et al. 2010), and binaries may have been affected by dynamical interactions before their release into the field (e.g., Ziosi et al. 2014).

We are grateful to the anonymous referee for constructive comments. We are also grateful to Vicky Kalogera for her helpful comments. This work was supported by NASA ATP Grant NNX14AP92G and NSF Grant AST1312945. S.C. also acknowledges support from the National Aeronautics and Space Administration through Chandra Award Number TM5-16004X/NAS8-03060 issued by the Chandra X-ray Observatory Center, which is operated by the Smithsonian Astrophysical Observatory for and on behalf of the National Aeronautics Space Administration under contract NAS8-03060.

## REFERENCES

Aarseth, S. J. 2010, Gravitational N-Body Simulations

—. 2012, MNRAS, 422, 841

Abbott, B. P., Abbott, R., Abbott, T. D., Abernathy, M. R., Acernese, F., Ackley, K., Adams, C., Adams, T., The LIGO Scientific Collaboration, & the Virgo Collaboration. 2016a, The Astrophysical Journal Letters, 818, L22

—. 2016b  
 —. 2016c, *Phys. Rev. Lett.*, 116, 241103  
 —. 2016d, *Phys. Rev. Lett.*, 116, 061102  
 —. 2016e  
 Altamirano, D., Patruno, A., Heinke, C. O., Markwardt, C., Strohmayer, T. E., Linares, M., Wijnands, R., van der Klis, M., & Swank, J. H. 2010, *ApJL*, 712, L58  
 Altamirano, D., Wijnands, R., Heinke, C. O., Sivakoff, G. R., & Pooley, D. 2012, *The Astronomer's Telegram*, 4264, 1  
 Antonini, F., Chatterjee, S., Rodriguez, C. L., Morscher, M., Pattabiraman, B., Kalogera, V., & Rasio, F. A. 2016, *ApJ*, 816, 65  
 Banerjee, S., Baumgardt, H., & Kroupa, P. 2010, *MNRAS*, 402, 371  
 Banerjee, S. & Kroupa, P. 2011, *ApJL*, 741, L12  
 Belczynski, K., Bulik, T., Fryer, C. L., Ruiter, A., Valsecchi, F., Vink, J. S., & Hurley, J. R. 2010a, *ApJ*, 714, 1217  
 Belczynski, K., Buonanno, A., Cantiello, M., Fryer, C. L., Holz, D. E., Mandel, I., Miller, M. C., & Walczak, M. 2014, *ApJ*, 789, 120  
 Belczynski, K., Dominik, M., Bulik, T., O'Shaughnessy, R., Fryer, C., & Holz, D. E. 2010b, *ApJL*, 715, L138  
 Belczynski, K., Kalogera, V., & Bulik, T. 2002, *ApJ*, 572, 407  
 Belczynski, K., Repetto, S., Holz, D., O'Shaughnessy, R., Bulik, T., Berti, E., Fryer, C., & Dominik, M. 2015, *ArXiv e-prints*  
 Bozzo, E., Ferrigno, C., Stevens, J., Belloni, T. M., Rodriguez, J., den Hartog, P. R., Papitto, A., Kreykenbohm, I., Fontani, F., & Gibaud, L. 2011, *A&A*, 535, L1  
 Brandt, W. N., Podsiadlowski, P., & Sigurdsson, S. 1995, *MNRAS*, 277, L35  
 Breen, P. G. & Heggie, D. C. 2013, *MNRAS*, 432, 2779  
 Carpenter, J. M. 2000, *AJ*, 120, 3139  
 Chatterjee, S., Fregeau, J. M., Umbreit, S., & Rasio, F. A. 2010, *ApJ*, 719, 915  
 Chatterjee, S., Rasio, F. A., Sills, A., & Glebbeek, E. 2013a, *ApJ*, 777, 106  
 Chatterjee, S., Rodriguez, C. L., Kalogera, V., & Rasio, F. A. 2016, arXiv:1609.06689  
 Chatterjee, S., Umbreit, S., Fregeau, J. M., & Rasio, F. A. 2013b, *MNRAS*, 429, 2881  
 Chernoff, D. F. & Weinberg, M. D. 1990, *ApJ*, 351, 121  
 Chomiuk, L., Strader, J., Maccarone, T. J., Miller-Jones, J. C. A., Heinke, C., Noyola, E., Seth, A. C., & Ransom, S. 2013, *ApJ*, 777, 69  
 Cordes, J. M., Romani, R. W., & Lundgren, S. C. 1993, *Nature*, 362, 133  
 de Boer, K. S., Tucholke, H.-J., & Schmidt, J. H. K. 1997, *A&A*, 317, L23  
 Dhawan, V., Mirabel, I. F., Ribó, M., & Rodrigues, I. 2007, *ApJ*, 668, 430  
 Djorgovski, S. & Meylan, G. 1994, *AJ*, 108, 1292  
 Dominik, M., Belczynski, K., Fryer, C., Holz, D. E., Berti, E., Bulik, T., Mandel, I., & O'Shaughnessy, R. 2012, *ApJ*, 759, 52  
 —. 2013, *ApJ*, 779, 72  
 Dominik, M., Berti, E., O'Shaughnessy, R., Mandel, I., Belczynski, K., Fryer, C., Holz, D. E., Bulik, T., & Pannarale, F. 2015, *ApJ*, 806, 263  
 Downing, J. M. B., Benacquista, M. J., Giersz, M., & Spurzem, R. 2010, *MNRAS*, 407, 1946  
 —. 2011, *MNRAS*, 416, 133  
 Fragos, T., Willems, B., Kalogera, V., Ivanova, N., Rockefeller, G., Fryer, C. L., & Young, P. A. 2009, *ApJ*, 697, 1057  
 Fregeau, J. M., Gürkan, M. A., Joshi, K. J., & Rasio, F. A. 2003, *ApJ*, 593, 772  
 Fryer, C. L. & Kalogera, V. 2001, *ApJ*, 554, 548  
 Gualandris, A., Colpi, M., Portegies Zwart, S., & Possenti, A. 2005, *ApJ*, 618, 845  
 Gürkan, M. A., Freitag, M., & Rasio, F. A. 2004, *ApJ*, 604, 632  
 Hénon, M. H. 1971, *Ap&SS*, 14, 151  
 Heggie, D. & Hut, P. 2003, *The Gravitational Million-Body Problem: A Multidisciplinary Approach to Star Cluster Dynamics*  
 Heggie, D. C. 1975, *MNRAS*, 173, 729  
 Hurley, J. R., Pols, O. R., & Tout, C. A. 2000, *MNRAS*, 315, 543  
 Hurley, J. R., Tout, C. A., & Pols, O. R. 2002, *MNRAS*, 329, 897  
 Irwin, J. A., Brink, T. G., Bregman, J. N., & Roberts, T. P. 2010, *ApJL*, 712, L1  
 Joshi, K. J., Nave, C. P., & Rasio, F. A. 2001, *ApJ*, 550, 691  
 Joshi, K. J., Rasio, F. A., & Portegies Zwart, S. 2000, *ApJ*, 540, 969  
 Kalogera, V., King, A. R., & Rasio, F. A. 2004, *ApJL*, 601, L171  
 King, I. 1962, *AJ*, 67, 471  
 King, I. R. 1965, *AJ*, 70, 376  
 —. 1966, *AJ*, 71, 64  
 Kowalska-Leszczynska, I., Regimbau, T., Bulik, T., Dominik, M., & Belczynski, K. 2015, *A&A*, 574, A58  
 Kroupa, P. 2001, *MNRAS*, 322, 231  
 Kroupa, P. & Boily, C. M. 2002, *MNRAS*, 336, 1188  
 Kulkarni, S. R., Hut, P., & McMillan, S. 1993, *Nature*, 364, 421  
 Kundu, A., Maccarone, T. J., & Zepf, S. E. 2002, *ApJL*, 574, L5  
 Lada, C. J. & Lada, E. A. 2003, *ARA&A*, 41, 57  
 Leigh, N. W. C., Lützgendorf, N., Geller, A. M., Maccarone, T. J., Heinke, C., & Sesana, A. 2014, *MNRAS*, 444, 29  
 Lewin, W. H. G. & van der Klis, M. 2006, *Compact Stellar X-ray Sources*  
 Lyne, A. G. & Lorimer, D. R. 1994, *Nature*, 369, 127  
 Maccarone, T. J., Kundu, A., Zepf, S. E., & Rhode, K. L. 2007, *Nature*, 445, 183  
 Mackey, A. D., Wilkinson, M. I., Davies, M. B., & Gilmore, G. F. 2008, *MNRAS*, 386, 65  
 Miller-Jones, J., Maccarone, T., Chomiuk, L., Strader, J., Bogdanov, S., Sivakoff, G., & Heinke, C. 2014a, *A new black hole candidate in the globular cluster 47 Tucanae*, ATNF Proposal  
 Miller-Jones, J., Maccarone, T., Chomiuk, L., Strader, J., Sivakoff, G., Heinke, C., Shishkovsky, L., & Huizinga, D. 2014b, *A comprehensive ATCA survey for black holes in southern globular clusters*, ATNF Proposal  
 Moody, K. & Sigurdsson, S. 2009, *ApJ*, 690, 1370  
 Morscher, M., Pattabiraman, B., Rodriguez, C., Rasio, F. A., & Umbreit, S. 2015, *ApJ*, 800, 9  
 Morscher, M., Umbreit, S., Farr, W. M., & Rasio, F. A. 2013, *ApJL*, 763, L15  
 Nelemans, G., Tauris, T. M., & van den Heuvel, E. P. J. 1999, *A&A*, 352, L87  
 Noyola, E. & Gebhardt, K. 2006, *AJ*, 132, 447  
 Pattabiraman, B., Umbreit, S., Liao, W.-k., Choudhary, A., Kalogera, V., Memik, G., & Rasio, F. A. 2013, *ApJS*, 204, 15  
 Pejcha, O. & Thompson, T. A. 2015, *ApJ*, 801, 90  
 Peters, P. C. 1964, *Physical Review*, 136, 1224  
 Pooley, D., Lewin, W. H. G., Anderson, S. F., Baumgardt, H., Filippenko, A. V., Gaensler, B. M., Homer, L., Hut, P., Kaspi, V. M., Makino, J., Margon, B., McMillan, S., Portegies Zwart, S., van der Klis, M., & Verbunt, F. 2003, *ApJL*, 591, L131  
 Porras, A., Christopher, M., Allen, L., Di Francesco, J., Megeath, S. T., & Myers, P. C. 2003, *AJ*, 126, 1916  
 Portegies Zwart, S. F. & McMillan, S. L. W. 2000, *ApJL*, 528, L17  
 Portegies Zwart, S. F., McMillan, S. L. W., & Gieles, M. 2010, *ARA&A*, 48, 431  
 Repetto, S., Davies, M. B., & Sigurdsson, S. 2012, *MNRAS*, 425, 2799  
 Repetto, S. & Nelemans, G. 2015, *MNRAS*, 453, 3341

Rodriguez, C. L., Chatterjee, S., & Rasio, F. A. 2016a, PhRvD, 93, 084029

Rodriguez, C. L., Haster, C.-J., Chatterjee, S., Kalogera, V., & Rasio, F. A. 2016b, ApJL, 824, L8

Rodriguez, C. L., Morscher, M., Pattabiraman, B., Chatterjee, S., Haster, C.-J., & Rasio, F. A. 2015, Physical Review Letters, 115, 051101

Rodriguez, C. L., Morscher, M., Wang, L., Chatterjee, S., Rasio, F. A., & Spurzem, R. 2016c, MNRAS, 463, 2109

Sana, H., de Mink, S. E., de Koter, A., Langer, N., Evans, C. J., Gieles, M., Gosset, E., Izzard, R. G., Le Bouquin, J.-B., & Schneider, F. R. N. 2012, Science, 337, 444

Sigurdsson, S. & Hernquist, L. 1993, Nature, 364, 423

Spera, M., Mapelli, M., & Bressan, A. 2015, MNRAS, 451, 4086

Spitzer, Jr., L. 1969, ApJL, 158, L139

Strader, J. 2014, A Black Hole in the Galactic Globular Cluster M10, Chandra Proposal

Strader, J., Chomiuk, L., Maccarone, T. J., Miller-Jones, J. C. A., & Seth, A. C. 2012, Nature, 490, 71

Strader, J., Miller-Jones, J., Maccarone, T., & Chomiuk, L. 2013, The ATCA Survey for Black Holes in Southern Globular Clusters, ATNF Proposal

Umbreit, S. 2012, Nature, 490, 46

Umbreit, S., Fregeau, J. M., Chatterjee, S., & Rasio, F. A. 2012, ApJ, 750, 31

Van Eck, S., Jorissen, A., Udry, S., Mayor, M., & Pernier, B. 1998, A&A, 329, 971

van Zyl, L., Charles, P. A., Arribas, S., Naylor, T., Mediavilla, E., & Hellier, C. 2004, MNRAS, 350, 649

Vink, J. S. 2008, NewAR, 52, 419

Vink, J. S., de Koter, A., & Lamers, H. J. G. L. M. 2001, A&A, 369, 574

Wang, C., Lai, D., & Han, J. L. 2006, ApJ, 639, 1007

Wang, L., Spurzem, R., Aarseth, S., Giersz, M., Askar, A., Berczik, P., Naab, T., Schadow, R., & Kouwenhoven, M. B. N. 2016, MNRAS, 458, 1450

Willem, B., Henninger, M., Levin, T., Ivanova, N., Kalogera, V., McGhee, K., Timmes, F. X., & Fryer, C. L. 2005, ApJ, 625, 324

Wong, T.-W., Valsecchi, F., Ansari, A., Fragos, T., Glebbeek, E., Kalogera, V., & McClintock, J. 2014, ApJ, 790, 119

Wong, T.-W., Valsecchi, F., Fragos, T., & Kalogera, V. 2012, ApJ, 747, 111

Ziosi, B. M., Mapelli, M., Branchesi, M., & Tormen, G. 2014, MNRAS, 441, 3703

Zuo, Z.-Y. 2015, A&A, 573, A58

**Table 2.** Initial model parameters.

No.	Name	$M$ ( $10^5 M_\odot$ )	$r_G$ (kpc)	$f_b$	$Z$	$r_v$ (pc)	BH-formation kick		High-mass Binaries			IMF	
							$\frac{\sigma_{\text{BH}}}{\sigma_{\text{NS}}}$	FB	$f_{b,\text{high}}$	$q$ range	$\frac{dn}{d\log P}$	range	$\alpha_1$
1	S	5.2	8	0.05	0.001	2	1	y	0.05	[0.1/ $m_p$ , 1]	$P^0$	[0.1, 100]	2.3
2	SR1Z	5.2	8	0.05	0.001	2	1	y	0.05	[0.1/ $m_p$ , 1]	$P^0$	[0.1, 100]	2.3
3	SR1	5.2	1	0.05	0.02	2	1	y	0.05	[0.1/ $m_p$ , 1]	$P^0$	[0.1, 100]	2.3
4	SR2	5.2	2	0.05	0.007	2	1	y	0.05	[0.1/ $m_p$ , 1]	$P^0$	[0.1, 100]	2.3
5	SR4	5.2	4	0.05	0.003	2	1	y	0.05	[0.1/ $m_p$ , 1]	$P^0$	[0.1, 100]	2.3
6	SR20	5.2	20	0.05	0.0003	2	1	y	0.05	[0.1/ $m_p$ , 1]	$P^0$	[0.1, 100]	2.3
7	SIwfb0.1	4.9	8	0.1	0.001	2	1	y	0.05	[0.1/ $m_p$ , 1]	$P^0$	[0.08, 150]	2.3
8	SIwfb0.1rv1	4.9	8	0.1	0.001	1	1	y	0.05	[0.1/ $m_p$ , 1]	$P^0$	[0.08, 150]	2.3
9	F0	5.2	8	0.05	0.001	2	1	y	0	-	-	[0.1, 100]	2.3
10	F1	5.6	8	0.05	0.001	2	1	y	1	[0.1/ $m_p$ , 1]	$P^0$	[0.1, 100]	2.3
11	F0.7Ms0.1	5.5	8	0.05	0.001	2	1	y	0.7	[0.1/ $m_p$ , 1]	$P^{-0.55}$	[0.1, 100]	2.3
12	F0.7q0.6	5.6	8	0.05	0.001	2	1	y	0.7	[0.6, 1]	$P^{-0.55}$	[0.1, 100]	2.3
13	F0.7q0.6R1	5.6	1	0.05	0.001	2	1	y	0.7	[0.6, 1]	$P^{-0.55}$	[0.1, 100]	2.3
14	F0.7q0.6R3	5.6	3	0.05	0.001	2	1	y	0.7	[0.6, 1]	$P^{-0.55}$	[0.1, 100]	2.3
15	K1	5.2	8	0.05	0.001	2	1	n	0.05	[0.1/ $m_p$ , 1]	$P^0$	[0.1, 100]	2.3
16	K2	5.2	8	0.05	0.001	2	0.1	n	0.05	[0.1/ $m_p$ , 1]	$P^0$	[0.1, 100]	2.3
17	K3	5.2	8	0.05	0.001	2	0.01	n	0.05	[0.1/ $m_p$ , 1]	$P^0$	[0.1, 100]	2.3
18	SIwfb0.1rv1K1	4.9	8	0.1	0.001	1	1	n	0.05	[0.1/ $m_p$ , 1]	$P^0$	[0.08, 150]	2.3
19	SIwfb0.1rv1K3	4.9	8	0.1	0.001	1	0.01	n	0.05	[0.1/ $m_p$ , 1]	$P^0$	[0.08, 150]	2.3
20	K1R1	5.2	1	0.05	0.02	2	1	n	0.05	[0.1/ $m_p$ , 1]	$P^0$	[0.1, 100]	2.3
21	K1R2	5.2	2	0.05	0.007	2	1	n	0.05	[0.1/ $m_p$ , 1]	$P^0$	[0.1, 100]	2.3
22	K1R4	5.2	4	0.05	0.003	2	1	n	0.05	[0.1/ $m_p$ , 1]	$P^0$	[0.1, 100]	2.3
23	K1R20	5.2	20	0.05	0.0003	2	1	n	0.05	[0.1/ $m_p$ , 1]	$P^0$	[0.1, 100]	2.3
24	K2R1	5.2	1	0.05	0.02	2	0.1	n	0.05	[0.1/ $m_p$ , 1]	$P^0$	[0.1, 100]	2.3
25	K2R2	5.2	2	0.05	0.007	2	0.1	n	0.05	[0.1/ $m_p$ , 1]	$P^0$	[0.1, 100]	2.3
26	K2R4	5.2	4	0.05	0.003	2	0.1	n	0.05	[0.1/ $m_p$ , 1]	$P^0$	[0.1, 100]	2.3
27	K3R1	5.2	1	0.05	0.02	2	0.01	n	0.05	[0.1/ $m_p$ , 1]	$P^0$	[0.1, 100]	2.3
28	K3R2	5.2	2	0.05	0.007	2	0.01	n	0.05	[0.1/ $m_p$ , 1]	$P^0$	[0.1, 100]	2.3
29	K3R4	5.2	4	0.05	0.003	2	0.01	n	0.05	[0.1/ $m_p$ , 1]	$P^0$	[0.1, 100]	2.3

*Table 2 continued*

Table 2 (*continued*)

No.	Name	$M$ ( $10^5 M_\odot$ )	$r_G$ (kpc)	$f_b$	$Z$	$r_v$ (pc)	BH-formation kick		High-mass Binaries			IMF	
							$\frac{\sigma_{\text{BH}}}{\sigma_{\text{NS}}}$	FB	$f_{b,\text{high}}$	$q$ range	$\frac{dn}{d\log P}$	range	$\alpha_1$
30	K3R20	5.2	20	0.05	0.0003	2	0.01	n	0.05	[ $0.1/m_p, 1$ ]	$P^0$	[0.1, 100]	2.3
31	K1R1Z	5.2	1	0.05	0.001	2	1	n	0.05	[ $0.1/m_p, 1$ ]	$P^0$	[0.1, 100]	2.3
32	K2R1Z	5.2	1	0.05	0.001	2	0.1	n	0.05	[ $0.1/m_p, 1$ ]	$P^0$	[0.1, 100]	2.3
33	K3R1Z	5.2	1	0.05	0.001	2	0.01	n	0.05	[ $0.1/m_p, 1$ ]	$P^0$	[0.1, 100]	2.3
34	FO.7Ms.0.1K1	5.5	8	0.05	0.001	2	1	n	0.7	[ $0.1/m_p, 1$ ]	$P^{-0.55}$	[0.1, 100]	2.3
35	FO.7Ms.0.1K2	5.5	8	0.05	0.001	2	0.1	n	0.7	[ $0.1/m_p, 1$ ]	$P^{-0.55}$	[0.1, 100]	2.3
36	FO.7Ms.0.1K3	5.5	8	0.05	0.001	2	0.01	n	0.7	[ $0.1/m_p, 1$ ]	$P^{-0.55}$	[0.1, 100]	2.3
37	FO.7q0.6K1	5.6	8	0.05	0.001	2	1	n	0.7	[0.6, 1]	$P^{-0.55}$	[0.1, 100]	2.3
38	FO.7q0.6K2	5.6	8	0.05	0.001	2	0.1	n	0.7	[0.6, 1]	$P^{-0.55}$	[0.1, 100]	2.3
39	FO.7q0.6K1R1	5.6	1	0.05	0.001	2	0.01	n	0.7	[0.6, 1]	$P^{-0.55}$	[0.1, 100]	2.3
40	FO.7q0.6K1R3	5.6	3	0.05	0.001	2	0.01	n	0.7	[0.6, 1]	$P^{-0.55}$	[0.1, 100]	2.3
41	FO.7q0.6K2R1	5.6	1	0.05	0.001	2	0.01	n	0.7	[0.6, 1]	$P^{-0.55}$	[0.1, 100]	2.3
42	FO.7q0.6K2R3	5.6	3	0.05	0.001	2	0.01	n	0.7	[0.6, 1]	$P^{-0.55}$	[0.1, 100]	2.3
43	Is	3.6	8	0.05	0.001	2	1	n	0.05	[ $0.1/m_p, 1$ ]	$P^0$	[0.1, 100]	3.0
44	If	16.1	8	0.05	0.001	2	1	n	0.05	[ $0.1/m_p, 1$ ]	$P^0$	[0.1, 100]	1.6
45	IsK1	3.6	8	0.05	0.001	2	1	n	0.05	[ $0.1/m_p, 1$ ]	$P^0$	[0.1, 100]	3.0
46	IsK2	3.6	8	0.05	0.001	2	0.1	n	0.05	[ $0.1/m_p, 1$ ]	$P^0$	[0.1, 100]	3.0
47	IsK3	3.6	8	0.05	0.001	2	0.01	n	0.05	[ $0.1/m_p, 1$ ]	$P^0$	[0.1, 100]	3.0
48	IfK1	16.1	8	0.05	0.001	2	1	n	0.05	[ $0.1/m_p, 1$ ]	$P^0$	[0.1, 100]	1.6
49	IfK2	16.1	8	0.05	0.001	2	0.1	n	0.05	[ $0.1/m_p, 1$ ]	$P^0$	[0.1, 100]	1.6
50	IfK3	16.1	8	0.05	0.001	2	0.01	n	0.05	[ $0.1/m_p, 1$ ]	$P^0$	[0.1, 100]	1.6
51	W	5.2	8	0.05	0.001	2	1	y	0.05	[ $0.1/m_p, 1$ ]	$P^0$	[0.1, 100]	2.3
52	WK1	5.2	8	0.05	0.001	2	1	n	0.05	[ $0.1/m_p, 1$ ]	$P^0$	[0.1, 100]	2.3
53	WK2	5.2	8	0.05	0.001	2	0.1	n	0.05	[ $0.1/m_p, 1$ ]	$P^0$	[0.1, 100]	2.3
54	WK3	5.2	8	0.05	0.001	2	0.01	n	0.05	[ $0.1/m_p, 1$ ]	$P^0$	[0.1, 100]	2.3
55	WF0.7q0.6	5.6	8	0.05	0.001	2	1	y	0.7	[0.6, 1]	$P^{-0.55}$	[0.1, 100]	2.3
56	WF0.7q0.6K1	5.6	8	0.05	0.001	2	1	n	0.7	[0.6, 1]	$P^{-0.55}$	[0.1, 100]	2.3
57	WIf	16.1	8	0.05	0.001	2	1	y	0.05	[ $0.1/m_p, 1$ ]	$P^0$	[0.1, 100]	1.6
58	WIfK1	16.1	8	0.05	0.001	2	1	n	0.05	[ $0.1/m_p, 1$ ]	$P^0$	[0.1, 100]	1.6
59	WIfK3	16.1	8	0.05	0.001	2	0.01	n	0.05	[ $0.1/m_p, 1$ ]	$P^0$	[0.1, 100]	1.6
60	Wrv1fb0.1	5.0	8	0.1	0.001	1	1	y	0.1	[ $0.1/m_p, 1$ ]	$P^0$	[0.08, 150]	2.3
61	Wrv1K1fb0.1	5.0	8	0.1	0.001	1	1	n	0.1	[ $0.1/m_p, 1$ ]	$P^0$	[0.08, 150]	2.3
62	Wrv1K3fb0.1	5.0	8	0.1	0.001	1	0.01	n	0.1	[ $0.1/m_p, 1$ ]	$P^0$	[0.08, 150]	2.3

NOTE—Each model initially has  $N = 8 \times 10^5$  stars. Column FB denotes whether or not natal kicks for BHs are dependent on fallback.  $\alpha_1$  denotes magnitude of the power-law exponent for stars of initial mass  $> 1 M_\odot$ .  $q$ -distribution is always uniform.

Table 3. Final structural properties of model clusters.

No.	t (Gyr)	$N$ ( $10^4$ )	$M$ ( $10^4 M_\odot$ )	$f_b$	$f_{b,c}$	$r_c$	$r_{c,\text{obs}}$ (pc)	$r_h$	$r_{hl,\text{obs}}$	$\rho_c$ ( $10^3 M_\odot/\text{pc}^3$ )	$\frac{v_{\sigma,c}}{v_{\sigma,c,\text{obs}}}$ (km s $^{-1}$ )		
1	12.0	71	26	0.05	0.05	2.90	3.06	7.89	5.55	17.8	1.9	9.8	3.40
2	$\approx 5$												
3	12.0	24	12	0.06	0.13	0.64	0.40	2.80	1.41	44.0	31.5	10.9	4.26
4	12.0	55	21	0.05	0.06	2.52	2.86	6.12	4.01	9.1	2.2	9.8	3.32
5	12.0	68	25	0.05	0.06	2.83	2.59	7.16	4.73	12.3	2.0	9.9	3.46
6	12.0	73	27	0.05	0.05	3.07	4.22	8.54	6.24	21.8	1.5	9.7	3.30
7	12.0	76	26	0.09	0.12	1.89	1.12	5.65	3.27	7.5	9.2	11.5	4.37

Table 3 *continued*

Table 3 (*continued*)

No.	t (Gyr)	N (10 <sup>4</sup> )	M (10 <sup>4</sup> M <sub>⊙</sub> )	f <sub>b</sub>	f <sub>b,c</sub>	r <sub>c</sub>	r <sub>c,obs</sub>	r <sub>h</sub>	r <sub>hl,obs</sub>	ρ <sub>c</sub> (10 <sup>3</sup> M <sub>⊙</sub> /pc <sup>3</sup> )	Σ <sub>c,obs</sub> (10 <sup>3</sup> L <sub>⊙</sub> /pc <sup>2</sup> )	v <sub>σ,c</sub> (km s <sup>-1</sup> )	v <sub>σ,c,obs</sub>
8	12.0	71	25	0.09	0.14	0.83	1.12	4.29	3.27	28.7	9.2	13.6	5.30
9	12.0	71	26	0.05	0.05	3.20	2.63	7.82	5.50	3.2	2.2	9.9	3.46
10	12.0	73	27	0.04	0.05	2.51	3.34	7.71	5.39	121.1	1.9	9.8	3.46
11	12.0	73	27	0.04	0.05	3.15	2.81	7.77	5.44	5.6	2.4	10.0	3.47
12	12.0	73	27	0.04	0.05	3.05	5.07	8.12	5.73	20.6	1.4	9.7	3.24
13	≈ 4									Dissolved			
14	12.0	63	24	0.04	0.05	3.05	2.24	7.54	5.25	14.0	2.4	9.2	3.23
15	12.0	77	28	0.04	0.11	0.36	0.22	4.98	2.47	275.1	126.6	14.2	6.08
16	12.0	76	27	0.05	0.07	2.00	1.42	5.71	3.48	8.3	7.6	11.7	4.38
17	12.0	70	26	0.05	0.05	3.09	3.73	8.20	5.90	9.1	1.3	9.7	3.30
18	12.0	69	23	0.08	0.13	0.32	0.22	4.56	2.17	371.1	121.3	14.9	6.41
19	12.0	69	24	0.09	0.12	1.41	1.12	5.00	2.90	68.7	122.9	12.1	4.64
20	12.0	30	14	0.05	0.14	0.20	0.17	3.05	1.30	678.2	126.0	12.0	4.92
21	12.0	66	25	0.04	0.12	0.37	0.05	4.54	2.02	226.6	2121.9	13.5	5.57
22	12.0	74	27	0.04	0.11	0.55	0.25	4.93	2.26	96.1	88.4	13.5	5.58
23	12.0	77	28	0.04	0.10	0.32	0.26	5.07	2.67	384.3	92.7	14.7	6.42
24	12.0	24	12	0.06	0.13	0.65	0.48	2.78	1.36	36.8	35.0	11.0	4.26
25	12.0	63	24	0.05	0.07	1.70	1.28	4.91	2.75	4.4	8.2	11.7	4.35
26	12.0	73	26	0.05	0.07	2.06	1.74	5.67	3.31	3.9	5.2	11.5	4.19
27	12.0	12	6	0.07	0.12	0.77	1.11	2.82	1.87	79.3	5.3	7.7	2.79
28	12.0	53	21	0.05	0.06	2.45	2.06	6.27	4.19	17.0	2.9	9.5	3.32
29	12.0	67	24	0.05	0.06	2.80	3.99	7.36	5.06	15.5	1.5	9.7	3.30
30	12.0	73	27	0.05	0.05	3.30	2.28	8.63	6.26	5.0	2.4	9.8	3.45
31	12.0	28	13	0.05	0.12	0.18	0.14	2.77	1.52	1124.2	205.1	13.7	5.78
32	12.0	20	10	0.06	0.09	1.02	1.44	2.89	1.92	13.9	8.1	9.7	3.39
33	≈ 4									Dissolved			
34	12.0	77	28	0.04	0.09	0.59	0.31	5.08	2.63	68.2	66.2	13.4	5.61
35	12.0	76	28	0.04	0.06	2.22	1.39	6.00	3.74	3.2	7.9	11.4	4.25
36	12.0	73	27	0.04	0.05	3.09	2.26	7.85	5.45	7.3	2.9	10.0	3.53
37	12.0	78	28	0.04	0.09	0.71	0.36	5.18	2.66	42.6	58.2	13.1	5.42
38	12.0	76	28	0.04	0.06	2.45	1.89	6.47	4.20	6.7	4.4	11.0	4.00
39	12.0	26	12	0.05	0.13	0.20	0.31	2.73	1.53	616.9	55.7	12.4	5.01
40	12.0	71	26	0.04	0.09	0.68	0.59	4.87	2.55	58.7	26.9	13.1	5.31
41	12.0	7	4	0.07	0.09	0.92	0.73	2.48	1.78	10.8	6.4	7.0	2.49
42	12.0	69	26	0.04	0.06	2.23	1.20	5.85	3.76	8.3	8.4	11.0	4.05
43	12.0	71	25	0.04	0.09	0.29	0.13	4.28	1.68	384.7	335.5	15.4	6.67
44	≈ 2									Dissolved			
45	12.0	74	25	0.04	0.07	0.21	0.18	4.63	2.06	966.6	175.1	13.5	5.85
46	12.0	72	25	0.04	0.08	0.20	0.14	4.46	1.97	1107.9	260.7	13.8	5.93
47	12.0	71	25	0.04	0.10	0.36	0.10	4.14	1.61	286.1	646.3	15.7	6.83
48	< 0.1									Dissolved			
49	≈ 3									Dissolved			
50	≈ 2									Dissolved			
51	12.0	69	25	0.05	0.05	3.58	4.72	8.57	6.17	3.7	1.1	9.3	3.10
52	11.0	77	28	0.04	0.10	0.56	0.26	4.73	2.31	89.7	112.1	14.5	6.06
53	12.0	74	27	0.05	0.06	2.50	1.57	6.28	4.07	2.6	5.8	11.0	4.05
54	12.0	63	24	0.05	0.05	3.96	7.76	10.55	7.95	10.4	0.5	8.2	2.58
55	12.0	69	26	0.04	0.05	3.64	2.20	8.38	5.90	2.4	2.4	9.4	3.31
56	12.0	77	28	0.04	0.09	0.76	0.56	5.09	2.61	34.4	35.1	13.3	5.49
57	≈ 0.6									Dissolved			
58	12.0	60	24	0.04	0.04	13.95	35.76	21.29	16.29	0.0	0.1	4.8	1.34
59	≈ 0.4									Dissolved			

Table 3 *continued*

Table 3 (continued)

No.	t (Gyr)	N (10 <sup>4</sup> )	M (10 <sup>4</sup> M <sub>⊙</sub> )	f <sub>b</sub>	f <sub>b,c</sub>	r <sub>c</sub> (pc)	r <sub>c,obs</sub> (pc)	r <sub>h</sub>	r <sub>hl,obs</sub>	ρ <sub>c</sub> (10 <sup>3</sup> M <sub>⊙</sub> /pc <sup>3</sup> )	Σ <sub>c,obs</sub> (10 <sup>3</sup> L <sub>⊙</sub> /pc <sup>2</sup> )	v <sub>σ,c</sub> (km s <sup>-1</sup> )	v <sub>σ,c,obs</sub>
60	12.0	67	23	0.09	0.12	1.86	1.16	5.33	3.15	5.7	10.7	11.4	4.36
61	12.0	64	22	0.09	0.13	0.36	0.14	3.56	1.61	647.6	9.2	17.0	7.27
62	12.0	65	23	0.09	0.11	2.42	1.46	6.50	4.24	5.7	253.7	10.3	3.79

NOTE—Serial numbers for models are the same as in Table 2. Observed structural properties are denoted by the subscript “obs.” Definitions for observed properties are explained in §3. The approximate dissolution times (§3.2) are listed for dissolved clusters.

Table 4. Properties of Black Holes.

No.	N <sub>BH</sub>	N <sub>BH,esc</sub>	N <sub>BH-BH</sub>	N <sub>BH-BH,esc</sub>	N <sub>BH-nBH</sub>	N <sub>BH-nBH,esc</sub>	N <sub>merge</sub>				M <sub>tot</sub>	
							z < 1 in	z < 1 out	z < 2 in	z < 2 out	z < 1 (M <sub>⊙</sub> )	z < 2 (M <sub>⊙</sub> )
1	464	1260	4	130	2	5	0	32	0	63	33.2 <sup>47.6</sup> <sub>23.8</sub>	44.2 <sup>49.3</sup> <sub>24.8</sub>
2	601	1001	2	97	1	2	0	17	0	46	34.7 <sup>46.7</sup> <sub>27.5</sub>	44.4 <sup>49.1</sup> <sub>28.5</sub>
3	165	1259	4	65	10	5	0	37	0	59	19.8 <sup>21.0</sup> <sub>8.8</sub>	19.9 <sup>21.5</sup> <sub>10.4</sub>
4	327	1213	4	132	2	1	0	42	0	83	26.7 <sup>30.5</sup> <sub>21.8</sub>	28.7 <sup>31.9</sup> <sub>22.4</sub>
5	393	1227	3	131	1	3	0	40	0	77	30.7 <sup>37.4</sup> <sub>24.0</sub>	31.5 <sup>37.4</sup> <sub>24.0</sub>
6	579	1200	4	146	1	6	0	45	0	80	32.0 <sup>44.9</sup> <sub>23.6</sub>	36.7 <sup>50.5</sup> <sub>24.0</sub>
7	139	1318	4	65	4	0	0	22	0	46	29.4 <sup>37.2</sup> <sub>20.0</sub>	32.2 <sup>38.6</sup> <sub>21.5</sub>
8	49	1458	6	103	4	11	0	32	0	55	21.6 <sup>34.7</sup> <sub>15.7</sub>	24.9 <sup>36.1</sup> <sub>15.7</sub>
9	458	1265	5	130	4	2	0	35	0	66	32.9 <sup>46.9</sup> <sub>26.7</sub>	40.8 <sup>49.7</sup> <sub>27.2</sub>
10	467	1286	3	156	1	37	0	39	0	68	35.4 <sup>48.3</sup> <sub>23.5</sub>	42.3 <sup>50.5</sup> <sub>21.2</sub>
11	437	1298	4	153	1	29	0	32	0	64	35.8 <sup>47.8</sup> <sub>25.9</sub>	41.8 <sup>50.7</sup> <sub>26.3</sub>
12	503	1367	2	159	2	23	0	42	0	66	35.7 <sup>50.8</sup> <sub>26.9</sub>	37.7 <sup>51.9</sup> <sub>23.9</sub>
13	686	1083	3	116	3	30	0	21	0	56	38.2 <sup>47.1</sup> <sub>25.2</sub>	41.0 <sup>50.8</sup> <sub>23.0</sub>
14	462	1346	3	151	4	32	0	44	0	75	32.1 <sup>50.9</sup> <sub>24.8</sub>	39.5 <sup>52.0</sup> <sub>24.3</sub>
15	6	1757	1	1	2	3	0	0	0	0	0.0 <sup>0.0</sup> <sub>0.0</sub>	0.0 <sup>0.0</sup> <sub>0.0</sub>
16	241	1465	3	89	2	0	0	25	0	49	28.1 <sup>45.6</sup> <sub>20.1</sub>	35.4 <sup>49.7</sup> <sub>20.4</sub>
17	759	967	3	138	5	2	0	50	0	71	34.9 <sup>49.5</sup> <sub>24.6</sub>	40.5 <sup>50.2</sup> <sub>24.7</sub>
18	1	1521	0	0	1	1	1	0	1	0	26.9 <sup>26.9</sup> <sub>26.9</sub>	26.9 <sup>26.9</sup> <sub>26.9</sub>
19	282	1218	4	172	6	11	0	52	0	102	19.6 <sup>29.6</sup> <sub>13.4</sub>	22.8 <sup>35.1</sup> <sub>14.1</sub>
20	0	1512	0	2	0	3	0	0	0	0	0.0 <sup>0.0</sup> <sub>0.0</sub>	0.0 <sup>0.0</sup> <sub>0.0</sub>
21	3	1637	1	0	0	2	1	0	1	0	11.6 <sup>11.6</sup> <sub>11.6</sub>	11.6 <sup>11.6</sup> <sub>11.6</sub>
22	3	1689	1	2	0	7	0	0	0	0	0.0 <sup>0.0</sup> <sub>0.0</sub>	0.0 <sup>0.0</sup> <sub>0.0</sub>
23	3	1797	0	2	1	7	1	0	1	0	37.5 <sup>37.5</sup> <sub>37.5</sub>	37.5 <sup>37.5</sup> <sub>37.5</sub>
24	132	1219	2	69	9	6	0	41	0	62	16.1 <sup>21.0</sup> <sub>10.7</sub>	17.6 <sup>21.3</sup> <sub>11.3</sub>
25	179	1345	2	80	3	2	0	25	0	54	25.6 <sup>30.7</sup> <sub>19.0</sub>	27.0 <sup>31.5</sup> <sub>20.0</sub>
26	239	1358	5	75	1	3	0	27	0	49	27.5 <sup>37.4</sup> <sub>19.3</sub>	31.4 <sup>37.5</sup> <sub>19.2</sub>
27	398	980	4	141	3	4	0	75	0	118	16.0 <sup>20.0</sup> <sub>12.0</sub>	17.1 <sup>20.3</sup> <sub>12.1</sub>
28	561	972	4	141	3	1	0	53	0	89	26.7 <sup>31.4</sup> <sub>20.0</sub>	27.4 <sup>31.5</sup> <sub>21.8</sub>
29	661	944	2	130	3	1	0	48	0	79	29.0 <sup>36.9</sup> <sub>21.9</sub>	31.2 <sup>37.4</sup> <sub>22.7</sub>
30	741	1046	7	145	1	5	0	43	0	76	30.3 <sup>48.0</sup> <sub>23.7</sub>	39.8 <sup>49.5</sup> <sub>24.0</sub>
31	1	1752	0	2	1	6	0	0	0	0	0.0 <sup>0.0</sup> <sub>0.0</sub>	0.0 <sup>0.0</sup> <sub>0.0</sub>
32	125	1418	3	81	1	4	0	36	0	51	27.9 <sup>48.0</sup> <sub>19.3</sub>	30.0 <sup>48.6</sup> <sub>19.7</sub>
33	881	671	3	94	3	1	0	20	0	51	36.2 <sup>48.0</sup> <sub>27.1</sub>	43.6 <sup>50.9</sup> <sub>27.7</sub>

Table 4 continued

Table 4 (*continued*)

No.	$N_{\text{BH}}$	$N_{\text{BH,esc}}$	$N_{\text{BH-BH}}$	$N_{\text{BH-BH,esc}}$	$N_{\text{BH-nBH}}$	$N_{\text{BH-nBH,esc}}$	$N_{\text{merge}}$				$M_{\text{tot}}$	
							$z < 1$		$z < 2$		$z < 1$	$z < 2$
							in	out	in	out	$(M_{\odot})$	
34	18	1732	2	20	5	41	0	3	0	3	$23.3_{16.9}^{35.9}$	$23.3_{16.9}^{35.9}$
35	279	1432	3	158	6	17	0	17	0	37	$30.0_{23.5}^{44.1}$	$38.1_{23.6}^{51.1}$
36	673	1020	3	190	3	13	0	46	1	74	$36.3_{23.5}^{50.9}$	$40.5_{23.7}^{51.1}$
37	31	1794	2	25	4	52	0	5	0	5	$22.9_{16.3}^{26.3}$	$22.9_{16.3}^{26.3}$
38	338	1498	3	215	3	18	0	32	1	55	$29.7_{21.2}^{41.3}$	$32.4_{18.4}^{50.8}$
39	13	1723	0	30	5	57	0	7	0	7	$19.6_{13.2}^{21.9}$	$19.6_{13.2}^{21.9}$
40	31	1795	3	28	5	61	0	3	0	3	$23.7_{22.6}^{25.9}$	$23.7_{22.6}^{25.9}$
41	176	1422	2	214	0	17	0	26	2	49	$26.9_{9.5}^{43.2}$	$28.3_{11.0}^{46.2}$
42	315	1449	5	208	6	14	0	34	0	65	$25.4_{19.3}^{46.9}$	$29.0_{19.0}^{49.6}$
43	1	165	0	13	1	2	0	2	0	4	$25.9_{23.5}^{28.3}$	$33.1_{23.7}^{46.7}$
44	1430	5377	2	185	5	25	0	38	0	105	$50.0_{21.8}^{53.3}$	$50.0_{23.7}^{53.4}$
45	0	169	0	0	0	1	0	0	0	0	$0.0_{0.0}^{0.0}$	$0.0_{0.0}^{0.0}$
46	0	165	0	9	0	2	1	1	1	5	$26.0_{25.0}^{26.9}$	$39.4_{25.2}^{49.3}$
47	4	164	1	24	0	3	0	4	0	12	$19.1_{15.7}^{24.7}$	$23.7_{15.8}^{47.9}$
48	61	19012	0	30	0	45	0	0	0	0	$0.0_{0.0}^{0.0}$	$0.0_{0.0}^{0.0}$
49	1452	7774	5	148	4	10	1	48	1	78	$49.2_{18.2}^{53.8}$	$49.6_{19.9}^{53.9}$
50	1557	2502	4	202	4	9	0	38	0	106	$49.9_{46.0}^{54.4}$	$50.0_{43.4}^{54.5}$
51	393	1341	2	139	3	10	0	36	0	69	$44.3_{32.0}^{55.3}$	$49.3_{32.2}^{55.4}$
52	1	1764	0	1	1	12	0	0	0	0	$0.0_{0.0}^{0.0}$	$0.0_{0.0}^{0.0}$
53	165	1563	3	103	1	3	0	29	0	52	$43.1_{32.0}^{63.3}$	$48.6_{33.1}^{68.0}$
54	653	1068	1	162	2	2	0	31	0	59	$49.7_{40.2}^{57.2}$	$51.0_{40.5}^{58.7}$
55	310	1761	3	282	3	103	0	24	0	55	$48.0_{36.4}^{54.2}$	$49.7_{27.3}^{74.9}$
56	21	1916	1	51	5	160	0	1	0	2	$60.2_{60.2}^{60.2}$	$67.6_{60.6}^{74.6}$
57	1500	8638	9	248	2	75	0	28	1	94	$54.6_{19.1}^{56.4}$	$54.8_{23.0}^{57.6}$
58	39	19134	0	43	17	143	0	0	0	0	$0.0_{0.0}^{0.0}$	$0.0_{0.0}^{0.0}$
59	1917	3554	11	322	4	13	0	14	0	117	$77.4_{35.1}^{82.0}$	$71.0_{19.8}^{84.7}$
60	54	1469	1	141	3	7	0	33	0	59	$33.6_{30.3}^{45.7}$	$36.2_{30.4}^{51.4}$
61	1	1519	0	1	1	25	3	0	3	1	$68.3_{59.7}^{74.6}$	$71.6_{59.9}^{79.5}$
62	289	1237	3	175	7	10	0	31	0	69	$34.3_{24.3}^{43.0}$	$36.2_{27.5}^{48.3}$

NOTE—Serial numbers for models are the same as in Table 2. Columns “in” and “out” denote BH-BH mergers inside and outside clusters. Number of BH-BH mergers and their total masses in the source frame are listed for  $z < 1$  and  $z < 2$  assuming  $z = 0 \equiv t = 12$  Gyr. The median and  $2\sigma$  ranges in total mass are listed.